Department of Precision and Microsystems Engineering

Design of a nanometer precision wavelength modulated interferometer

W.P.C. van de Sande

Report no : OM-2021.069
Coach : Dr. L.A. Cacace
Professor : Ir. J.W.Spronck
Specialisation : Opto-Mechatronics
Type of report : Master Thesis
Date : 30-09-2021

Abstract

A wavelength modulated interferometer is presented, based on a telecom laser source. A solution for the target distance dependency of wavelength modulated interferometers is presented. With the introduction of a delay line, the modulation depth variation is reduced. A method and a sensor head for the reduction of the thermal dependency of this delay line are presented. The resulting interferometer has sub-nanometer non linearity errors and a thermal dependency of below 3 nmK^{-1} with a working range of 1 meter.

Contents

1 Introduction

1.1. The need for fiber fed interferometers

In the semiconductor industry, there is a trend for a ever-decreasing feature size, as a result, the acceptable overlay errors need to reduce as well. At the moment the overlay is in the order of nanometers. To accomplish these requirements a precise position measurement system is necessary [8, 19].

As the accuracy and precision of Displacement Measuring Interferometry (DMI) can be in the order of nanometers it has become an important technology for feedback or error measurements [10]. DMI can also be advantageous as it can provide an accurate non-contact measurement with a high dynamic range [6].
A disadvantage of DMI is the required laser head which often produces a significant amount of heat. This heat can cause errors in the system. Spatially separating the laser source from the rest of the machine can help to reduce the effects of this heat on the performance of the system. However, the alignment of the laser source with respect to the measurement optics needs to be stable. As a result, there is a strong interest in fiber fed DMI where the source light is transmitted through a fiber towards the measurement head, providing a flexible way to deliver the light to the required location without introducing a sensitivity to fiber deformations. [10].

1.2. Existing solution at Prodrive Technologies

Prodrive Technologies (PT) operates in the semiconductor industry as a research, development and production partner. In this industry high precision metrology is crucial and an in-house solution is being developed. The goal of this development is to create a demonstrator for the developed technology which exists as a proof of concept. This proof of concept demonstrates the ability of the algorithm and electronics to determine a displacement of a retroreflector over a small range for a single measurement axis. The demonstrator should be a sensor head which has specifications comparable to commercial interferometers to demonstrate that this technology is feasible for practical applications. The interferometer is based on wavelength modulation comparable to as is described in [50]. The principles and considerations regarding this demodulation scheme are explained in2.3.1. Advantages of this solution are the use of a low cost laser source in the form of a telecom laser diode. a further advantage of this laser source is the long lifetime, which reduces machine downtime due to a laser replacement.

1.3. Goal and outline

The goal is to design a fiber fed displacement measurement interferometer based on quadrature demodulation with non linearity errors which are smaller or comparable to commercially available heterodyne interferometers.
In chapter 2 some interferometer principles are explained to provide some background information about DMI and the used principle for quadrature detection. in chapter 3 the system requirements are discussed and explained. In chapter 4 error sources present in interferometers based on the wavelength modulation are discussed. Then in chapter 5 the principle of a delay line to reduce the dependency of the modulation depth on the measured distance is presented together with some practical considerations. Hereafter the conceptual design for the sensor head is discussed in detail in chapter 6, by discussing some methods to achieve

the required performance and then presenting multiple concepts of which the most suited is selected. In chapter 7 this concept is designed in detail together with the the delay line. The errors are budgeted and an alignment plan is presented. Lastly, the conclusions are presented and recommendations are done for further work.

2

Interferometer principles

In this chapter the most important principles used in a wavelength modulated DMI are discussed. First the basic layout of the most used interferometer type is discussed. Then two different approaches to extract displacement information from the interference signal are discussed and the approach used in the proof of concept is explained in more detail.

2.1. Basic layout

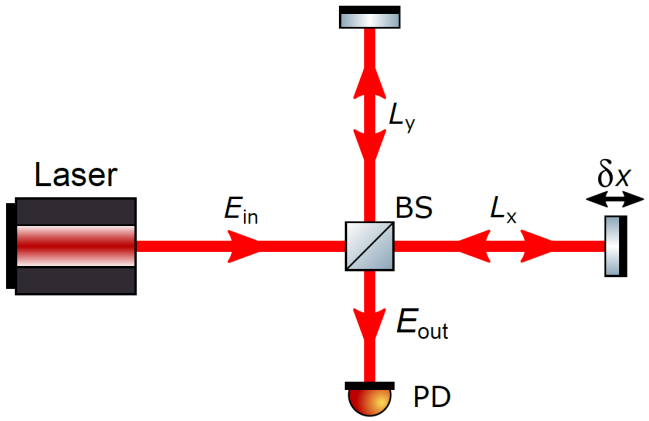

Figure 2.1: A schematic layout of a Michelson interferometer. Light is emitted by a laser source, and split by the beamsplitter (BS) the light in each arm of the interferometer is reflected by a mirror and travels back to the beamsplitter where both signals are combined. A part of this combined signal travels to the photodiode (PD). The intensity measured at the photodiode depends on the difference in optical path length between both measurement arms [53].

An often used interferometer type for DMI is a Michelson interferometer. The basic components of a Michelson interferometer are a light source, a beamsplitter, two mirrors and a detector [11].
The light source is typically a collimated, coherent light source such as a laser. This collimated light is directed at a beamsplitter which splits the light in two measurement branches, both directed towards a mirror. The light reflects of the mirror and is directed back to the beam splitter where both signals combine and produce an interference signal. This intensity of this signal is dependent on the relative phase difference between the measurement branches and is picked up by a photodetector. Many DMI sensor heads can be seen as a variation of the Michelson interferometer.

With this setup a displacement can be determined by counting the amount of fringes that are seen at the photodetector, however it is not possible to determine the direction of travel. Furthermore, interpolating within a single wavelength is not unambigiously possible as there are multiple points within a single wavelength with the same signal.

Without further measures this setup is not suitable to determine a displacement unambiguously.

2.2. Homodyne and Heterodyne

To create ambiguity in the measurement different methods can be used, these can be classified as homodyne detection and heterodyne detection.

A homodyne interferometer uses a single frequency laser source whereas a heterodyne interferometer uses a two frequency laser source [11]. In a homodyne interferometer the displacement of a mirror is determined by counting the number of fringes seen in the interference signal, the speed can be determined by determining how many fringes are seen per unit of time. However the direction of the displacement can not yet be determined from this information as the signal is the same for a mirror moving away or towards the sensor. The interference signals amplitude is a sinusoidal function of the relative phase difference between the two interfering signals. If a 90° phase shifted interference signal can be created as a second signal, two sinusoidal signals are generated of which one leads the other. With these two signals the phase between two fringes can be extracted unambigiously and the direction of the displacement can be extracted. This is called quadrature detection and will be discussed in 2.3.

A Heterodyne interferometer uses a two frequency light source to create a beat frequency which is much lower than the optical frequency and is accessible by photodetectors. The phase difference between the original signals can directly be extracted from this beat signal [11]. If one of the two frequency components is Doppler shifted by the reflecting off a moving mirror the beat frequency changes and the velocity of the movement can be extracted by electronically comparing the measured beat frequency with the beat frequency between the two original frequencies emitted by either the laser or a frequency modulator [31].

For both methods there are considerations which place constraints on the design of a sensor head. For example a homodyne interferometer needs quadrature detection to determine the direction of travel which can introduce its own errors. In heterodyne interferometers the presence of two signals can introduce errors due to unwanted signal mixing, this is especially of concern in fiber based interferometers[19]. As the laser source used in the proof of concept is a single wavelength laser source the following chapters focus on homodyne systems.

2.3. Quadrature detection

The generation of two signals that are in quadrature can be done in different domains. A well known solution is the optically generated quadrature signals. Such as retarding one polarization state of the reference signal to create a phase shifted interference signal in one polarization direction and a not phase shifted signal in the other polarization direction. A polarizing beam splitter (PBS) is then used to separate both signals and detect each signal [53]. An example is shown in figure 2.2. The quadrature signals can also be generated electronically if the laser is modulated. These signals can be extracted after detection by demodulation the interference signal. The considerations for this method and the working principle are discussed in the next section.
Two signals in quadrature are often shown in a lissajous signal where one signal is the x value and the second is the y value. If the signals are in perfect quadrature the signal describes a circle where the angle is the phase difference. The effect of errors on this signal is described in 4.2.3.

2.3.1. Wavelength modulation

To extract the phase of the interference signal the wavelength can be modulated. The wavelength is modulated with a sinusiodal input signal around a central peak. By using lock in demodulation at the modulation frequency a signal proportional to the derivative of the fundamental interference signal can be extracted. As the derivative of a sinusoidal signal is a 90° shifted sinusoidal signal these two signals can be used to detect the quadrature of the signal. The amplitude of these sinusoidal signals is proportional to respective Bessel function which are dependent on the modulation depth. The modulation depth is dependent on the optical path difference between the two interference signals according to 2.1[51].

$$\delta\Phi = \frac{2\pi\Delta x n_{medium}\delta\lambda}{\lambda^2} \tag{2.1}$$

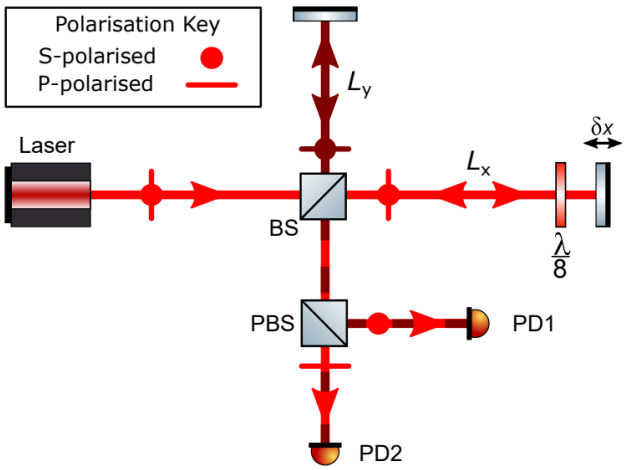

Figure 2.2: A schematic of a simple optical quadrature detector the $\lambda/8$ waveplate has its fast axis aligned with one polarization state. By double passing this waveplate one polarization state is retarded a quarter wave creating quadrature signals. [53]

Where $\frac{\delta\lambda}{\lambda^2}$ is the modulation of the laser Δx is the path difference and n is the refractive index of the medium. If the modulation depth varies an unequal gain non linear error arises, this is explained in more detail in section 4.2.3. If the modulation depth is not constrained then the relevant Bessel function can cross zero, and no signal is retrieved. This is also the case if the modulation depth approaches zero. The first three Bessel functions are shown in figure 2.3, it can be seen that the magnitude of the J_0 and J_1 are equal at approximately 1.4 rad. This is the optimal modulation depth for a system with a DC signal and a signal demodulated at the modulation frequency. For a system which uses the demodulation at the modulation frequency and demodulation at two times the modulation frequency the optimal modulation is the crossing of the J_1 and J_2 terms.

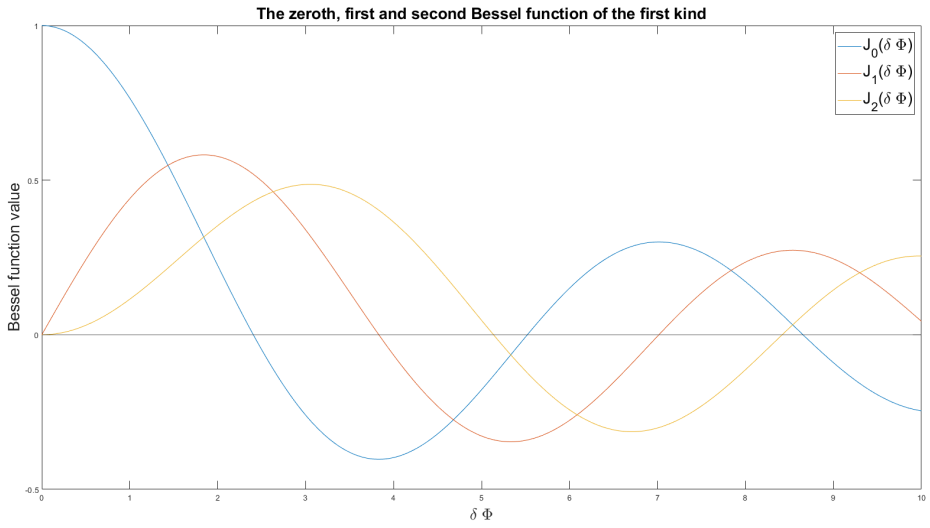

Figure 2.3: The three first Bessel functions of the first kind

For a system with only one sensor head connected to the laser source the modulation of the laser can be adapted to control the modulation depth. And if a non zero path difference between the interfering signals is integrated by design a minimum modulation depth can be build in the system.
However, for multiple independent sensor heads which may all have a different measurement distance laser modulation control can not guarantee the optimal modulation depth for each sensor head. A second problem arises if a differential sensor head is used. With a differential setup a point with zero path difference can be

within the desired operating range of the sensor.

Wavelength control
The wavelength stabilization uses the wavelength modulation to lock to an absorption peak in a gas cell. Since the demodulated signal is proportional to the derivative of the intensity with respect to the wavelength this signal can be used to determine where on the absorption peak the current center wavelength is located as long as the current center wavelength is close to the center wavelength of the absorption peak. This information can be used to control the center wavelength by controlling the temperature of the laser diode. The modulation of the wavelength is done by modulating the current through the diode.

3

System Requirements and nice to haves

To give a start point for the design first the requirements need to be defined. The system requirements are split up in different parts: performance requirements, requirements regarding configurations and requirements regarding working environment. Performance aspects as well as features which are not required but nice to have are also presented.
For the input of the performance requirements an overview of some commercially available interferometers is shown to determine the ballpark for the requirements for the interferometer.

Interferometer	Renishaw RLD10	Zygo HSPMI	Attocube	Smaract picoscale	Keysight 10706B
Non linearity error [nm]	< 1	1	n.s.	< 6	n.s.
Repeatability [nm]	n.s.	n.s	2	n.s	n.s
Working distance [m]	1	1	5	5	n.s
Thermal error [nm/°C]	< 50	< 18	n.s	n.s	<40
Maximum target speed [m/s]	1	2.1	2	1	2.7
Reference	[30]	[57]	[4]	[35]	[18]

Table 3.1: Some specifications of other commercial interferometers, note that not some specifications are dependent on the used combination of optics and electronics such as maximum target speed or range. Not all specifications are determined at the same working distance or target speed. The best specifications are shown here. For the Zygo and Keysight interferometers the non linearity errors and the thermal errors are giving for the optics only, for the other systems no such distinction is available and the these errors are specified for the entire system.

The interferometer demonstrator is designed to work on a stage demonstrator. The requirements for this interferometer are partly based on the specifications in the state of the art for interferometers and the motion of the stage demonstrator. The goal of the project is to show the working principle of the interferometer and demonstrate that the errors are better or equal to the state of the art.

3.1. Performance requirements

3.1.1. Working distance

The longest stroke of the stage demonstrator is 420 mm. The interferometer range shall exceed this to provide some freedom in the mounting. A range of 500 mm is satisfactory for this application.

3.1.2. Target speed

The maximum speed of the demonstrator stage is below 1 m/s. For this requirement it is choosen to create a comparable requirement with some commercial interferometers to show that the interferometer is competitive.

Parameter	value
Working Distance	0-500 mm
Target speed	1 m/s
Target angle	200 µrad
Repeatability	1 nm
Non linearity error	1 nm
Signal stability [2.5 s]	200 pm
Thermal drift	< 50 nm/°C
Lifetime	> 10 year
Wavelength	1550 nm

Table 3.2: Requirements on the performance of the system, the repeatability and stability are given for 2σ

3.1.3. Target angle

The acceptable target rotation of the demonstrator is based on the yaw error motion of some stages with comparable size to the demonstrator stage used in precision applications and the demonstrator stage. The stages noted in table 3.3 are examples of off the shelf available stages. In most cases where an interferometer is used for position measurement lower error motions are expected. However the acceptance angle should exceed the error motions of these stages as that might increases the number of potential use cases for the interferometer. As a result the permissible target angle for the interferometer demonstrator is choosen to

Stage	Aerotech – PlanarDLA	Aerotech - PlanarHDX	PI - V-741 PIMag	PI - A-322 PIglide HS
Pitch [µrad]	87	10	3	2
Roll [µrad]	87	10	60	10
Yaw [µrad]	48	5	n.s.	n.s.
Reference	[2]	[3]	[27]	[26].

Table 3.3: Some stages with their respective pitch, roll and yaw error motions.

be 200 µrad to cope with an error motion of the stage. As this angle is relative small compared to assembly tolerances an adjustable mount with an incremental motion in the order of 50 µrad should be used to mount and align the interferometer.

3.1.4. Repeatability

The repeatability is defined as the difference in measured distance as the target moves away from one position and returns to this position during a continuous measurement. The repeatability shall be maximum ± 1 nm. The repeatability is defined at a constant temperature and excludes errors due to thermal variations during measurement. The value of 1 nm is choosen as this is in the same order of magnitude of the commercial heterodyne interferometers.

3.1.5. Non linearity error

The uncorrectable non linearity error of the interferometer shall be below 1 nm. Non linearity errors which can be corrected can be greater than this.

3.1.6. Signal stability

In the proof of concept with lab equipment the signal stability is proven to be 200 pm. The demonstrator shall have at least the same short term signal stability as the proof of concept despite adding more features.

3.1.7. Thermal drift

The error due to thermal variations of the environment and the sensor shall be below 50 nm. This is the same order of magnitude for multiple interferometers in the state of the art. The temperature of a controlled environment can be controlled to the order of 10 mK [1] for high precision environments. For a variation lower than 20 mK the thermal error is lower than the systems repeatability.

3.1.8. Lifetime
The lifetime of the components used at a conceptual level in demonstrator shall exceed 10 years continuous operation. This is required as a feature of demonstrator is a long mean time before failure for the laser source. It is hard to qualify for a lifetime and to verify if this requirement will be met, however during the design process care shall be taken to exclude short lifetime components.

3.2. Configurations and features
In this section requirements on the configuration and the features of the interferometer are described.

3.2.1. Plane mirror target
The target of an interferometer can be a retro reflector or a plane mirror, for a retroreflector a translation ortogonal to the measurement direction translates the returning beam at twice this translation. As a result a retroreflector is only a suitable target for a measurement of an object that only moves in a single translational degree of freedom in the direction of the measurement. Typical stages have multiple translational degrees of freedom, to measure these translations with a retroreflector target the measurements should be stacked and the sensors should move together with the target for the orthogonal translations. As a result the interferometer may not be able to detect some error motions of the stage.

For a parallel measurement of a multiple degree of freedom stage a target translation orthogonal to the measurement direction should not effect the signal strength, therefore a plane mirror shall be used as a target.

3.2.2. Alignment
For the alignment of the sensor head with respect to a mounting frame a way of aiding the alignment shall be presented. This may be in the form of a "rough" and "fine" alignment procedure. These procedures shall be able to indicate how to align the sensor and converge to a aligment such that the sensor fulfills the other requirements.

3.2.3. Modulation depth independent axes
The interferometer design must incorporate a method to make the modulation depth approximately independent of the target distance, to solve the problem presented in section 2.3.1.

3.3. Working environment
The working conditions are specified for the sensor head of the interferometer. The light source and signal processing can be placed in an ambient environment.

3.3.1. Temperature and Humidity
The sensor head shall be able to perform in a lab or temperature controlled production environment.

Parameter	value
Temperature	15 - 35 °C
Humidity	0-95% non condensing

Table 3.4: Requirements on the working environment

3.3.2. Vacuum compatibility
Fluctuations in the refractive index of air present errors in the distance measurement of a DMI. As a result interferometers are often used in a low pressure environment. For qualification of the interferometer some test may be carried out in a vacuum chamber, the interferometer should work in an environment with low pressure, however as there is no use case specified for the demonstrator the outgassing of used materials is not constrained.

3.4. Lead time component availability
Due to commercial planning the demonstrator shall be built and tested as soon as possible. As a result the lead time for the components, and especially the optical components shall be as short as possible. In the

design the lead time shall be minimized by choosing readily available components over custom components if possible.

3.5. Nice to have

3.5.1. Extended range

It is preferred to have a range that extends to 1 m distance as that would make the demonstrator compatible for more use cases.

3.5.2. Sensor size

It is preferred to keep the sensor head in a size comparable or smaller than 50 mm x 50 mm x 110 mm.

3.5.3. Vacuum connections

It is preferred to have as little optical vacuum feedthroughs as there is often a limited quantity available in a customer product as well as in the vacuum chamber available for testing

3.5.4. Product costs

For the demonstrator the design does not need to be optimized for low cost production, however it is preferred to keep the bill of materials under €20000 for a single sensor head.

4

Errors in homodyne displacement interferometers

4.1. Environmental error sources

4.1.1. Thermal errors

The optical path length (OPL) depends on the refractive index of the traversed medium and the distance through that medium. The refractive index is dependent on the temperature. For most materials this is a positive relation, so a higher temperature gives a higher refractive index. For thermal expansion this is also the case, most materials expand upon heating. Both effects combine to the thermo-optic behaviour of the material, which describes the relation between the optical path length and the temperature. For some materials such as fused silica the optical path change due to temperature is dominated by the change of refractive index, and for other materials such as calcite the thermal expansion dominates the optical path change. [29].

As an interferometer measures the relative phase difference between two signals it measures the difference in optical path length. If there is a mismatch in glass length or material properties between both optical paths the measurement is sensitive to a temperature change. This effect is used in for instance fiber temperature sensors to detect the temperature such as [7]. An ideal DMI should not operate as a temperature sensor as these displacements can not be distinguished from a target displacement.
For birefringent materials used in for example waveplates the thermal effect on the optical path can introduce other errors. In a waveplate light polarized in one direction travels a longer optical path to introduce retardance with respect to light polarized in the othogonal direction due to a different refractive index for each polarization direction. The optical path length through the birefingent material is such that a specific amount of retardance is introduced. If the waveplate is used at another temperature the optical path length is different and the retardance can be effected [9], the magnitude of this effect depends on the design and material of the waveplate.

4.1.2. Refractive index variation of air

As an interferometer measures the optical path difference between two paths it is sensitive to anything that the optical path length is sensitive to. The optical path length can be described by equation 4.1.2 where l is the geometric path length, n is the local refractive index and ds is the infinitesimal small local part of the geometrical path.

$$OPL = \int_l n ds \tag{4.1}$$

If the local refractive index changes the measured OPL changes as well, therefore the measurement is sensitive to the changes in the refractive index of the medium. The refractive index changes with the temperature, humidity, pressure and composition of the air so the measurement is sensitive to any changes in the environment. A method of compensating for these errors can be the use of a weather station, where different parameters are measured and the effect on the refractive index of air can be calculated by for instance Cid-

dor's equation or the modified Edlen's equation, where the latter is most often used as it is more accurate at environmental conditions typically seen in a lab or production environment [56]. The accuracy of both of these equations is typically limited by the accuracy in the measurement of the environmental conditions. For typical laboratory conditions the extended uncertainty is approximately $2 * 10^{-8}$ [56], which would result in an uncertainty of 10 nm for the maximum target distance of 500 mm.

Another method of determining the refractive index of air is the use of a refractometer, a method where a differential measurement is done between a vacuum tube and the path through the air outside that tube. This method can be used to determine the refractive index of air to an uncertainty of $1 * 10^{-8}$ [20].

Both methods do not compensate for local changes in the refractive index of air which for instance can be the result of turbulence.

4.2. Non linearity Errors

Non linearity errors are the result of influences that create non linearity in the measured distance. Often these error sources produce cyclic errors. Some error sources producing non linearity are mixing of signals, ghost reflections and quadrature detection errors [14, 53].

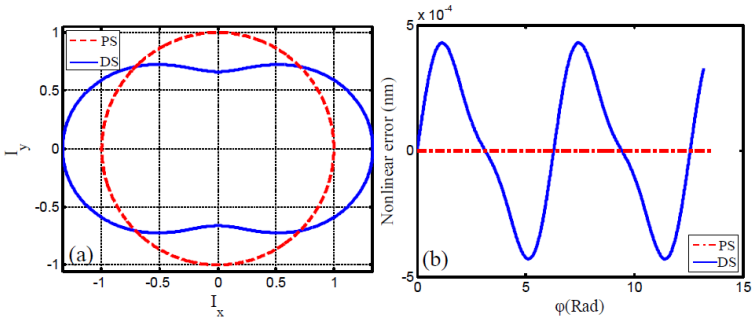

Figure 4.1: An example of a non linear error and its effect on the lissajous figure [14]. PS is the perfect signal and DS is the distorted signal.

4.2.1. Signal mixing

If parts of the optical path are common for both the measurement and the reference beam in a location where they need to be distinguishable from each other unwanted signal mixing can occur. This is often encountered in double pass systems where an optical component is passed multiple times by each beam. If the signals are separated by polarization state an imperfection in a polarization dependent component can create mixing of signals [5]. For instance a polarizing beam splitter has a finite extinction ratio for the reflected and transmitted polarization state, as a result the signal separation is not perfect and signal mixing can occur. For absorptive polarizers this is also the case, however the extinction ratio for an absorptive polarizer is typically higher than that of an reflective polarizer which can be used as a beamsplitter. Birefringent waveplates have a finite retardance accuracy, as a result the relative phase shift between the fast and slow axis can be slightly different than predicted. If a quarter wave plate is used to create a circular polarization state this polarization state can be elliptical in some form due to the finite accuracy.

4.2.2. Ghost reflections

An unwanted reflection off an interface in the sensor head that reaches the detector can introduce a non linear error as this reflection creates additional interference signals. These interference signals are referred to as Parasitic Interference Signals (PIS). These interference signals can be the interference between a desired signal and a ghost reflection, but also between different ghost reflections. [14] The first order ghost reflections have a much higher intensity if components without an anti-reflection coating are used.

4.2.3. Quadrature errors

In homodyne interferometers with an optical quadrature detector three intrinsic non linear errors arise. The first is an unequal gain between the detectors. As the phase shifted signal is detected by a different detector

an unequal gain between the detectors creates a deviation from a circle in the Lissajous signal in which the phase is measured. An example is shown in figure 4.2.

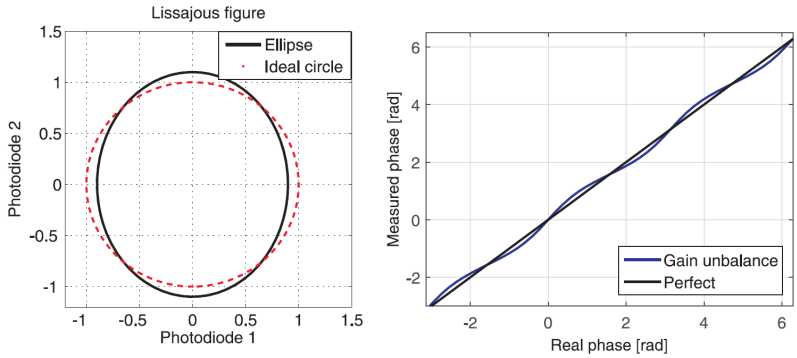

Figure 4.2: The signal resulting from an unequal or unbalanced gain of two detectors [53].

The second error is a phase shift between the signals that is not exactly 90°, then the signals are not exactly in quadrature. In an interferometer with an optical quadrature detector this phase shift is introduced in a waveplate. Any imperfection in this waveplate results in a different phase relation between the two measured signals. An example is shown in figure 4.3.

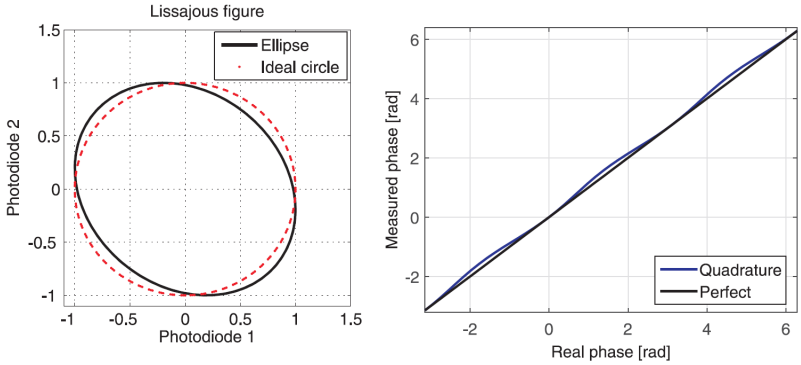

Figure 4.3: The signal resulting if the two measured signals are not exactly in quadrature [53].

The third error is a DC offset on any of the detectors, such an offset must be compensated before the phase can be extracted as the center of the lissajous figure shifts with this offset. An example is shown in figure 4.4. These errors can be compensated to some extend. [13]
For wavelength modulating interferometers the quadrature signals are dependent on the modulation depth as described in section 2.3.1. As a result the detector gain is dependent on the measured distance and must be actively compensated. Often this correction is done by fitting the measured signal to the unit circle [21].

4.3. Moving target errors

A Doppler shift of the reflected light due to a moving target mirror creates light of a frequency that differs from the original frequency. Due to this difference in frequency and thus wavelength the phase of the interference between these two signals also depends on the common distance after reflection and not only the difference in distance. If the common distance is constant this error can be corrected for by calibration, however if this distance is varying with temperature, as would happen if for instance a long fiber is part of this common distance, this can introduce not compensable errors.

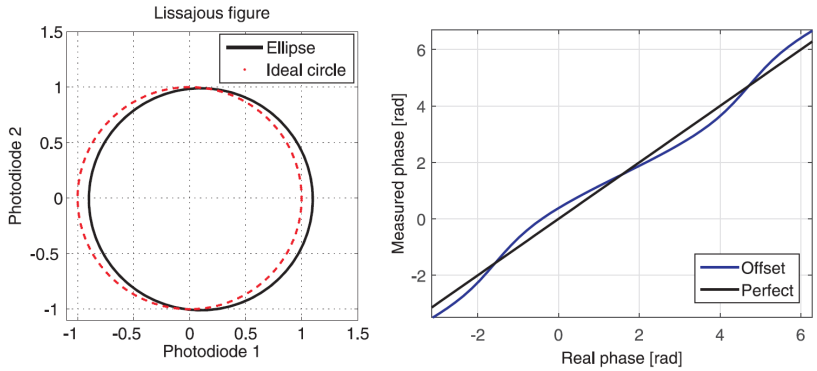

Figure 4.4: The resulting signal if one of the detectors has an offset [53].

5

Delay line

In figure 5.1 the Bessel functions to which the quadrature signals are proporional are shown. If the laser modulation is controlled such that for one master sensor head the modulation is at the crossing of these two functions the difference in distance measured by the other sensors with respect to the master sensor needs to be small compared to the distance measured at the master sensor. As a result the working range of the other

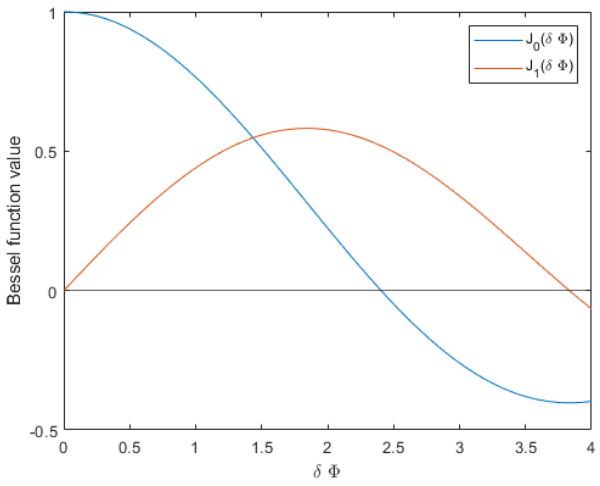

Figure 5.1: The J_0 and J_1 Bessel functions of the first kind. The measured quadrature signals are proportional to these functions, and the $\Delta\Psi$ is proportional to the optical path difference for a constant laser modulation.

sensors is small and changes with the measured distance of the master sensor. Therefore, the measurement axis are not independent. A delay line can be used to reduce this dependency, this will be explained in the rest of this chapter.

5.1. Delay line concept

If a delay line is introduced in such a way that the variation in modulation depth in the working range of the interferometer is small compared to the modulation depth introduced by the delay line the laser modulation can be kept constant.

However, with the introduction of a delay line some other practical issues are introduced. As the delay line is part over the interference experiment any deviation in length of the delay line cannot be distinguished from a movement of the target. Secondly, the modulation of the laser source should be decreased by the same factor as the path length difference increases by the delay line to keep the same modulation depth at the detector, the laser modulation is also used for the wavelength control, so decreasing the laser modulation to much may harm the wavelength stability.

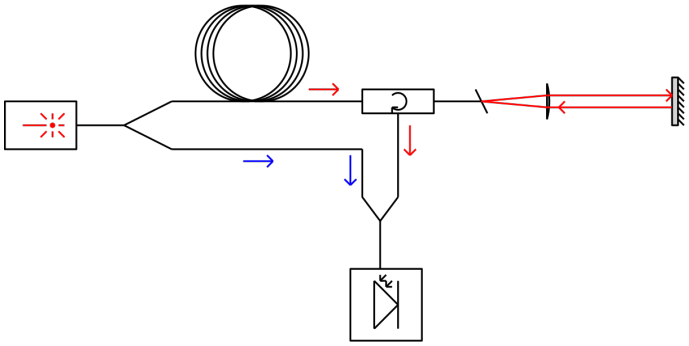

Figure 5.2: An example of a delay line. The red signal travels through the delay line and towards the target mirror and is interfered with a second signal that has travelled through a shorter fiber creating a difference in path length between both signals.

5.1.1. Thermal stability

To create a thermal stable sensor either the delay line must be made thermally stable or the variation of the delay line must be measured such that the distance measurement can be compensated for variations in the delay line.

As the delay line length must at least be in the same order of magnitude as the maximum target distance the delay line would be in the order of meters. Keeping this thermally stable to within 50 nm/°C requires a knowledge of the CTE of the materials within 10^{-8} and a temperature measurement with the same precision. However, if the optical length of the delay line can be measured with the same precision as the distance is measured the drift of the delay line can be compensated in the measurement data and no strict requirements would be posed on the thermal behaviour of the delay line delay line.

To determine the change of optical path length in the delay line a second interference experiment can be done, one between a signal that has travelled through the delay line and a second signal that has not travelled through the delay line but through the second path and a second interference experiment between the signal that has travelled through the delay line and to the target mirror and a the same second signal that has travelled through the second fiber. Subtracting the distance measured in the first experiment from the distance measured in the second experiment yields the difference between the reference and the target mirror. By doing two measurements the electric noise of the photodiode is also measured twice.

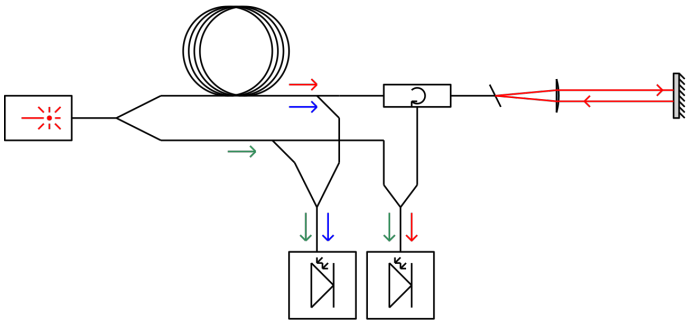

Figure 5.3: An example of a setup where a delay line is introduced and two interference experiments are done, one measuring the length change of the delay line with respect to the other fiber and one which measures the difference between a signal that has travelled through the delay line and towards a target mirror and a signal that has travelled through the second fiber. This example is not thermally stable for the parts after the fiber splitters but shows the application of a measured delay line.

5.1.2. Wavelength stabilisation

The delay line can not be chosen arbitrarily long as a longer line requires a smaller laser modulation for the same modulation depth at the detector. The relation between the total target distance and the laser modulation is given by equation 2.1.

A longer distance in the interference signal would require an inverse proportional lesser wavelength modulation, which creates reduces the signal for the wavelength stabilization. Therefore the delay line should be

as short as possible while still creating sufficient range for the target. The wavelength stabilisation is proven to be sufficient with a 25 Torr gas cell. Decreasing the modulation depth would require a decrease of the absorption line width in the gas cell, this can be possible by using a lower pressure gas cell, in section 7.1.6 this will be expanded further.

5.2. Practical considerations

Multiple configurations can be used to create a delay line, for instance a free space solution in the sensor head can be created, or the delay line can be created outside the sensor head.

Inside sensor head

A delay line placed inside the sensor head can be advantageous as only one signal is delivered by fiber towards the sensor head and the necessary delay is generated inside the sensor head, however the creation of such a delay line would increase the size of the sensor head. The delay line must at least be in the same order of magnitude as the target distance, requiring multiple passes of a cavity or a very long cavity. This cavity may expand due to thermal variations as the displacement of the cavity is measured, however this displacement should vary in a continuous manner as a discrete step such as a variation in the number of cavity passes is not measured correctly by the interferometer. If the amount of reflections in the cavity changes due to for instance thermal expansion this step is not detected.

Outside sensor head

A delay line can also be created before the sensor head, in the control unit or in the fiber leading towards the sensor head. For the control unit, with the laser and the electronics onboard there are no strict size requirements as this can be placed at a remote location however it is still advantageous to keep the delay line compact. If the delay line is created outside the sensor head two signals should be delivered to the sensor head, a delayed signal and a not delayed signal.

In fiber

For the delivery of these two signals by fibers two solutions are possible, two signals through one fiber separated by polarization or two distinct fibers each guiding one signal. The advantages of a single fiber are ease of alignment for the collimation of the light as only a single fiber needs to be aligned and both signals are parallel by default. Furthermore only a single fiber as input saves space in both the sensor head and the necessary ports in a vacuum chamber. A disadvantage of separation by polarization in a single fiber is the limited extinction ratio, and the sensitivity of the extinction ratio to environmental and mechanical influences[24].

With two distinct fibers no signal mixing can occur as the signals are spatially separated. The delay can be introduced by increasing the length of one of the delivery fibers with respect to the other delivery fibers. By rolling the fiber the size of this extra fiber can be contained inside the control unit. With this setup the light path before the sensor head is contained inside fibers and fiber based components entirely, increasing the stability of these components.

5.3. Conclusion

An in fiber delay line of which the thermal expansion is measured is deemed to be the most practical form of a delay line as the laser delivery is already via fiber. A long fiber can be coiled on a spool inside the control unit reducing the size of the claim of the delay line. The two signals will be delivered via two separate fibers as this solution eliminates sources for signal mixing in the beam delivery.

6

Conceptual design Sensor head

In this chapter, the conceptual design for a sensor head with a delay line will be discussed. First, some required functions together with embodiments for these functions will be discussed, after which different concepts which contain some of these solutions will be discussed. A qualitative ghost refection and crosstalk analysis with an estimate of the magnitude of each error source will be performed for each concept to aid in the concept selection.

Two distance measurements are required inside the sensor head. These two measurements comprise four lightpaths: a measure path, red in figure 6.1, comprising a lightpath from the laser source via a delay line towards the target and then to the photodetector, a first reference path, blue in figure 6.1, comprising the light path from the laser source via the delay line to reference mirror and then to a second photodetector and two second reference paths, green in figure 6.1, comprising a light path from the laser source via a second fiber to both of the two photodetectors. The second reference paths are common for most part of the distance traveled, at the least specifically within the fibers. Ideally any distance except the target distance (i.e. the distance between the sensor head and the target mirror) and the reference distance (the distance between the sensor head and the reference mirror) is common between either the measure distance and the first reference distance, the measure distance or first reference distance and its respective second reference path or between both second reference paths.

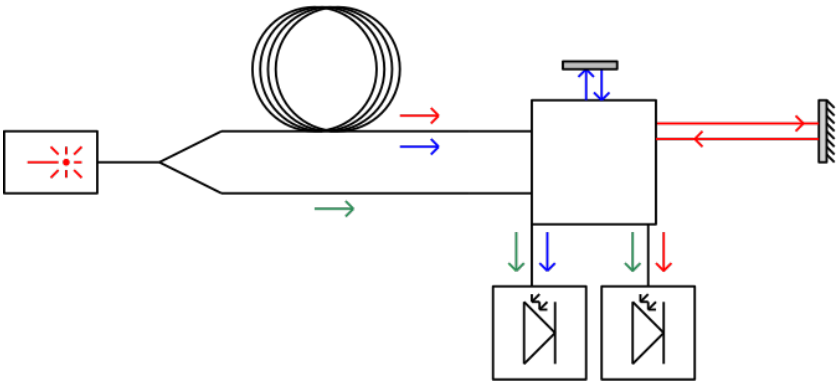

Figure 6.1: A schematic representation of which signals should travel through the sensor head, the red signal is the measure path, the blue signal is the first reference path and the green signal is the second reference path.

6.1. Functions and features of the sensor head

In this section the methods to create the required features in the sensor head are discussed. First methods for signal separation are discussed, hereafter a method to accommodate a plane mirror target is discussed and lastly, methods to reduce the thermal sensitivity of the sensor head are discussed.

6.1.1. Separation of signals

To separate any signals traveling a common path different properties of the signal can be used: the polarization state, the wavelength, and the direction of travel. A fourth method of separation can be a spatial separation, the path is not common, but if the distance traveled is equal and changes in the same way due to external influences, so the spacing between the signals is small the distance can be considered common. For each method of signal separation sources of signal mixing and typical considerations will be discussed.

Polarization separation

Two signals can be separated by polarization state if their polarization states are orthogonal. Signal mixing can occur due to a finite extinction ratio in polarizing components, due to an error in retardance in waveplates, misalignments of the polarization-dependent components with respect to each other and due to unwanted polarization effects in non polarizing components such as stress birefringence or retardance and diattenuation at interfaces with different refractive indices.

Stress birefringence can occur in glasses due to internal stresses resulting from the melting process [32] but it can also be introduced if the optics are overconstrained. The last effect can be mitigated if the polarization state is linear and aligned with the local p or s polarization state of the interface. Every optical component can have an effect on the polarization state of the light. For instance, a reflection can introduce diattenuation and retardance in the signal. And every polarization-dependent component can be considered imperfect. These effects and imperfections may lead to mixing of the signals.

Wavelength separation

If the signals have a different wavelength dichroic mirrors, dispersive optics and wavelength filters can be used to separate signals that have traveled a common path. Either a special laser source, two distinct laser sources, or frequency modifying optics such as acousto-optic frequency shifters or second harmonic generators are necessary to generate two wavelengths. Signal mixing can occur due to non perfect transmission or reflectance for the respective wavelength. Furthermore, unlike polarization, the wavelength of the light might not be changed as straightforward as the polarization state.

Direction separation

Two signals can also travel the same path but in a different direction. This method of separation is particularly sensitive to ghost reflections as a reflection changes the direction of travel. If the ghost reflection of a first signal is aligned with the signal traveling the opposite direction the reflection cannot be distinguished from the second signal. All interfaces with a different refractive index may create ghost reflections.

Spatial separation

If the signals do not overlap but are separated spatially signal mixing can be prevented. [15] presents an approach to create an interferometer with no detectable cyclic non linear error using this principle. A schematic of the differential sensor head is shown in figure 6.2, the other sensor heads presented in this paper use the same principles but suffer from a higher thermal instability. The downside of spatially separating the signals

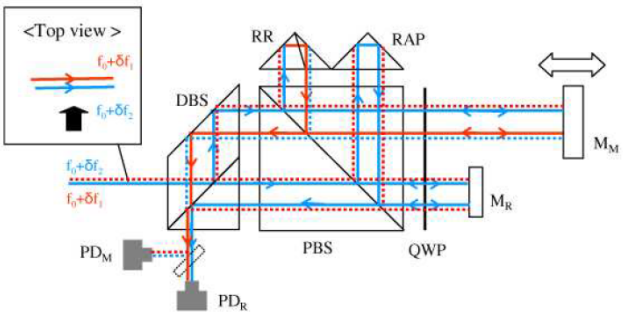

Figure 6.2: A differential interferometer with spatial signal separation to achieve no periodic non linearity errors [16]. The spatially separated signals are mixed as one signal travel throug a retroreflector (RR) which displaces the signal in a direction perpendicular to the plane of the drawing and the other signal through a right angle prism (RAP) which does not displace the signal in that direction.

is a sensitivity to thermal gradients and an increase in size.

6.1.2. Plane mirror target

If the plane mirror target is tilted the reflected wavefront is tilted at twice the target rotation, this may cause a decrease of the contrast of the interference at the photodiode. If a double pass setup is created where the target mirror is only used to fold the lightpath towards a retroreflector the wavefront tilt is reversed in the second reflection of the target mirror. In this case, only a lateral displacement wavefront at the detector is the result of a rotating target mirror, this is called beam shear. This beam shear also causes a loss of contrast, for a double pass setup the beam shear is twice the beam shear present in a single pass configuration. The contrast loss due to beam shear can be minimized by using a wider beam.

The second advantage of a double pass setup is that the optical resolution increases as well, so a 1 nm displacement gives a change of 4 nm traveled path for the light instead of 2 nm for a single pass.

A disadvantage of a double pass can be the higher perceived speed of the target, which reduces the maximum target speed which can be measured with a given ADC frequency.

For a double pass setup, two elements are required, a retroreflector to retroreflect the ray back to the target mirror and a method of inserting the signal and extracting the signal of the cavity created by the retroreflector and the plane mirror.

Retroreflectors

Two well-known embodiments for a retroreflector are the cube corner retroreflector and the cat's eye retroreflector. A cube corner retroreflector (CCR) consists of three reflective surfaces, each perpendicular to the other two. A light ray that reflects off all three surfaces is retroreflected back in its original direction.

In a cube corner the linear polarization of the incoming light can not be aligned with the s or p polarization state of all the reflections as there are three reflections in different directions.
There are two different variations of a CCR, one works with total internal reflection (TIR), and the other works with a reflection of a metallic surface. The last one can be a metal-coated solid glass CCR or a hollow CCR consisting of three mounted mirrors.
TIR introduces retardance between the local s and p polarization resulting in an elliptically polarized output for a linear polarized input [12]. If retardance effects can be cancelled a TIR CCR might be suitable for polarization preservation as there is no diattenuation. In [22] a solution with a phase compensated coating where the retardance effects are cancelled is presented. The resulting polarization is almost linear with a a 0.2° azimuth and a 0.1° ellipticity.

A metalized CCR tends to preserve the polarization better than a TIR CCR [17]. However a metalic CCR still introduces retardance and diattenuation of the polarization states [12], this diattenuation is dependent on the tilt and orientation angle of the incoming beam. Using the Mueller matrix for the preferred polarization preserving CCR the ratio between the major and minor axis of the elliptical polarization can be computed.[17] For linearly polarized light with a 1550 nm wavelength the resulting ellipticity is 0.26°.

As a cube corners comprises three reflections it is in principle not sensitive to variations of wavelength, only the refraction on the entrance surface of a solid CCR is sensitive to dispersion, however this does not effect the angle of the returning light.

A cat's eye retro reflector consists of a focusing optic such as a lens and a reflecting mirror. If the mirror is placed at the focal plane of the lens the incoming light is retro reflected back in the original direction. Different configurations with focussing lenses or mirrors are possible. [36, 38] A cat's eye retroreflector works with only one reflection off which the angle of incidence is a design parameter. As the retardance and diattenuation are dependent on the incidence angle this gives some design freedom. This can create a retroreflector that is polarization preserving [25]. If the linear polarization states are aligned with the local p and s polarization of the reflection any diattenuation or retardance does not effect the polarization of the signal.

Configurations of a double pass

Some possible configurations for a double pass sensor head will be discussed to introduce the working principles.

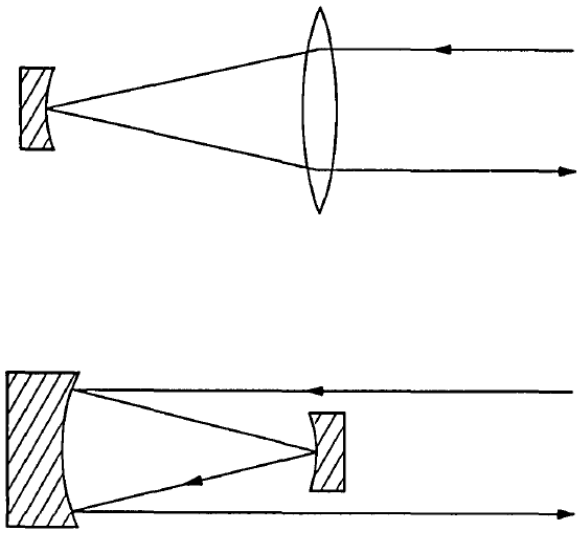

Figure 6.3: An example of two schematic configurations of a cat's eye retroreflector [36].

A configuration with a polarizing beamsplitter, quarter waveplate and a retroreflector can be used, for instance as is shown in 6.4 this solution is refered to as a High Stability Plane Mirror Interferometer (HSPMI) Another solution could be to use a retroreflector which itself acts as a beamsplitter such that the light can

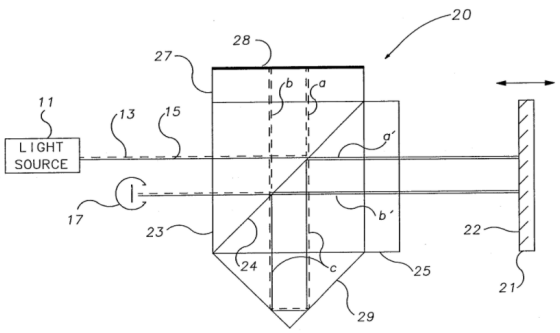

Figure 6.4: The high stability plane mirror interferometer. 13 and 15 both represent one signal of the light emitted by the light source 11, these signals are polarized orthogonal with respect to each other. 24 is the polarizing beam splitting coating reflecting signal 13 and transmitting signal 15. 25 and 28 both are quarter waveplates with their fast axis oriented at 45°, this creates circular polarization for both signals. 21 and 28 are the target mirror and reference mirror respectively and due to the reflection off these mirror the circular polarization changes handedness. This light travels back through the quarter waveplates where it is now orthogonally polarized with respect to its original polarization direction. The signal that was reflected by the polarizing beam splitter is now transmitted and vice versa. Both signals retroreflect in the cube corner and travel the same path backwards with only an offset due to the cube corner. In the last pass both signals are combined at the beamsplitting coating and travel to the detector 17. [55].

pass the retroreflector on the way in, and after double passing the cavity exits the retroreflector.

A variation on this embodiment is presented in [50] . The retroreflector in this design is a cat's eye configuration with the collimator lens and the fiber ferrule as a mirror. If the target angle is small the sensor head works as a single pass option and the reflected light is coupled back into the fiber but if the target angle is larger the cavity is passed twice. This is illustrated in figure 6.5. There are two problems that arise in this setup, the first is that the amount of passes is dependent on the target angle so if the target rotation varies the measured distance switches between double and single pass, which has an effect on the continuity of the measurement, the optical resolution and the modulation depth of the measurement.

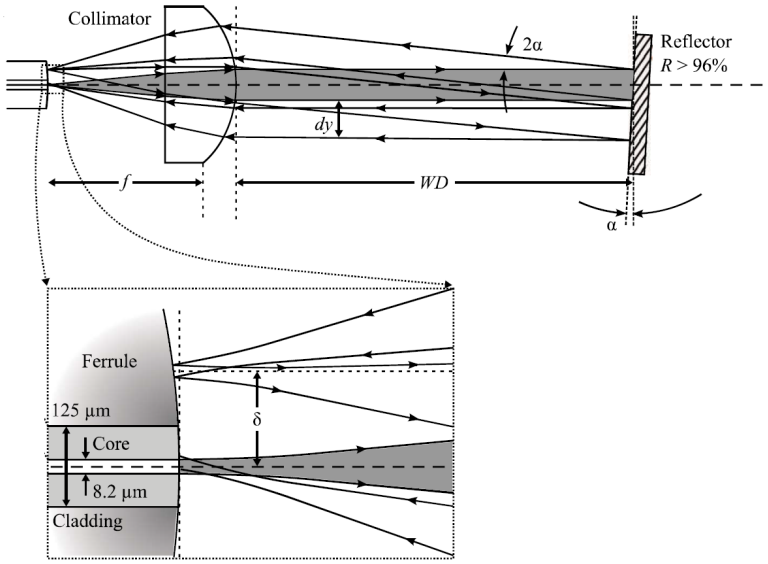

Figure 6.5: The compact sensor head in double pass operation [50]. If δ approaches zero the returning signal enters the fiber core creating a single pass configuration.

The second problem in this setup is the finesse of the cavity, the mentioned sensor head works with a low finesse cavity, in a double pass option the attenuation of the cavity per pass should be half the attenuation of the single pass cavity. This changes the contrast of the measurement significantly decreasing the resolution for at least one of the two principles.

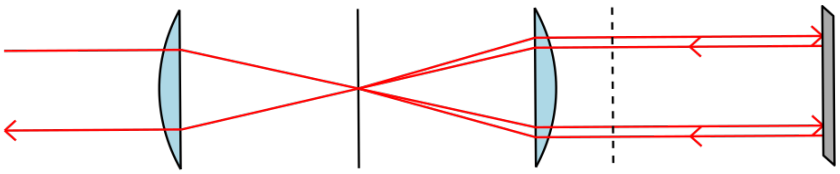

Figure 6.6: A cat's eye retroreflector with a reflective polarizer as mirror. The left lens focusses the light on the polarizer so that the second lens collimates the light coming from this focus. After passing through the quarter wave plate (dashed) the light is circularly polarized. Upon reflection off the target mirror the handedness of the polarization changes, as a result the light is linear polarized, rotated 90°with respect to the first linear polarization state.

A cat's eye retroreflector with a reflective polarizer as mirror can be used to create a retroreflector with an integrated beamsplitter, an example is shown in figure 6.6. In this setup the double pass configuration is again created by separating the signals by polarization state.

6.1.3. Thermally balanced

The sensor head should not act as an temperature sensor so the internal optical path length of the measurement path and the reference path should change equally for a uniform temperature change. Three distinct situations can be identified which are all thermally balanced in a uniform environment but can be more or less sensitive to thermal gradients. The first is a common overlaying path, this is the most stable situation as any expansion of the respective section is equal for both signals, not only for a uniform temperature change, but also for a temperature gradient. The second is a spatially separated parallel path, the signals travel the same distance through glass and are not sensitive to a thermal gradient along the travel direction but they are sensitive to thermal gradients perpendicular to the travel direction. The third situation is a situation where the signals travel an equal amount of distance through a different piece of glass, such as a in the PBS in the HSPMI illustrated in figure 6.4. In this situation the sensitivity to gradients is dependent on the configuration, and the sensitivity to a homogeneous temperature change is effected by the tolerances on the different pieces of glass, the last effect is typically very small so this configuration can be used to correct for homogeneous temperature variations.

6.2. Concepts

In this section four concepts are presented, each using a different combination of methods for creating a thermally balanced double pass configuration as required for a plane mirror.

6.2.1. HSPMI inspired

The first concept is a variation of the HSPMI suitable for working with a delay line, with a cat's eye retroreflector instead of a cube corner retroreflector.

Signal path

The first signal comprising the measurement and first reference signal enters the sensor head at the bottom fiber end, it is collimated by a collimator lens placed in front of this fiber end. The collimated lightbeam enters the first polarizing beamsplitter (PBS1) at an off center location. In the first polarizing beamsplitter the first signal is separated in the measurement signal and a first reference signal. Each signal travels twice to the target mirror (TM) and the reference mirror (RM) respectively. They are double passed in the same manner as is described in the HSPMI configuration (figure 6.4). After the double pass both signals exit PBS1 at another off center location in the same face they entered the PBS1. The measurement signal and first reference signal travel a common path where they are separated by polarization state. In the second polarizing beamsplitter (PBS2) the target beam and the first reference beam are separated and each travel to a different photodiode. The second signal enters the sensor head at the left fiber end after which it is collimated and enters PBS2. In PBS2 the second signal is separated in two portions, each combining with the measurement signal and the first reference signal respectively. The portion of the second reference that is combined with any one of the measurement or reference signal is polarized ortogonal with respect to the signal it is combined with, to create interference a linear polarizer (Pol1 or Pol2) is placed with its polarization axis such that both signals have the same polarization. The specific angle of this polarizer can be choosen such that both signals have an equal amplitude.

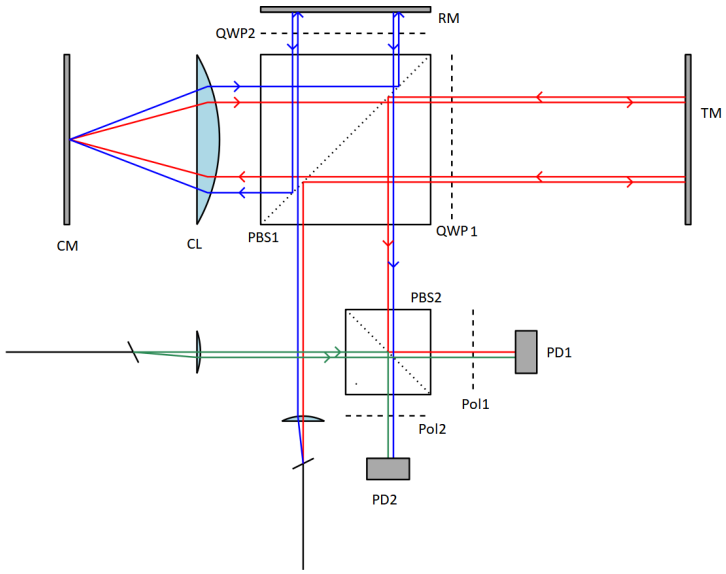

Figure 6.7: The HSPMI inspired sensor head, which is suitable for working with the proposed delay line, a cat's eye retroreflector consisting of a lens (CL) and a mirror (CM) replaces the CCR in this concept to reduce sources for signal mixing.

Error sources

In the presented concept some signal mixing due to polarization errors can reach the photodetector. Two first single ghost reflections and two single polarization errors reach the photodetector for each interference measurement. Both the internal and external ghost reflections off the outer surface of the quarter waveplate are directly mixed with the measure or first reference signal. The lightpath of one of these ghost reflections is depicted in figure 6.8. By placing the QWP at such an angle that the resulting signal travels off axis and does not reach the photodetector this source of ghost reflections can be deminished. However placing the QWP at an angle may deteriorate the performance of the QWP, so the angle should be minimal. An alternative can be

to place the QWP at such an angle that the modulation of the interference generated by the ghost reflection is minimal, for a short distance travelled this rotation is typically smaller than the rotation required to move the signal away from the photodiode, therefore reducing the effect on the retardance of the QWP.

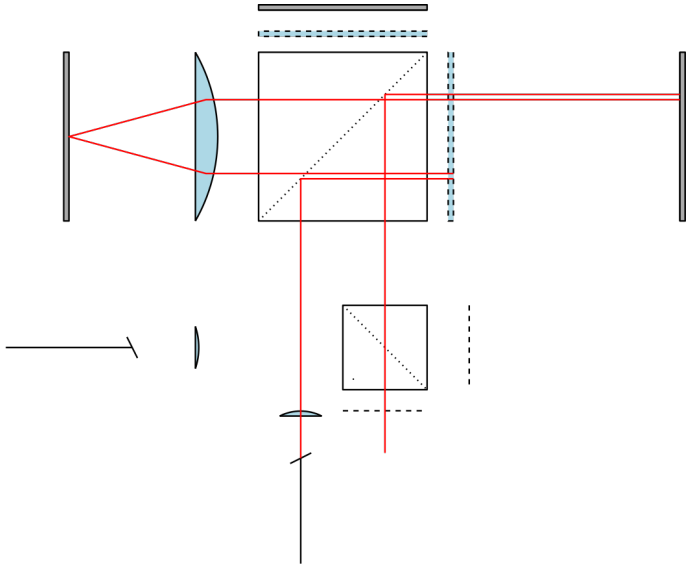

Figure 6.8: A first order ghost reflection that reaches the photodetector, this reflection is also present in the reference signal (top mirror)

For signal mixing due to polarization crosstalk there are only two signals that reach the photodetector for polarization errors due to a single element. A change of the polarization state inside the retroreflector creates a signal that first travels to one mirror (e.g. the target mirror) and in the second pass travels to the other mirror (e.g. the reference mirror) and then travels to the photodetector. The cat's eye retroreflector can be configured such that either the local p or s polarization states are aligned with the linear polarization state of any of the signals, then the effect due to retardance and diattenuation does not cause an error.

The second source of polarization crosstalk is the imperfect polarization separation inside the PBS2. This directly mixes a portion of the first reference with the measurement signal and vice versa. However, the interference phase of the parasitic signal with the second reference is known from the other interference experiment. So if the magnitude of the crosstalk can be determined during a calibration step this error source can be compensated for.

Crosstalk due to two imperfect polarization optics can also reach the photodetector. The signal of which the polarization is not rotated exactly 90° by the double pass through the QWP and that is transmitted by PBS1 due to a finite extinction ratio travels the same path as the the polarization crosstalk in figure 6.9. The same is the case for the crosstalk due to the finite extinction ratio of PBS1 at the third pass and again an imperfect polarization rotation by the second double pass of the QWP.

The crosstalk due the the finite extinction ratio in PBS1 in the fourth pass or the polarization aberration in the double pass of the QWP in the last pass sends the signal back through the retroreflector, the finite extinction ratio in the subsequent second pass through PBS1 or a polarization aberration in the double pass of the QWP combines this signal with the original signal.

Extinction ratios are typically defined as a ratio of intensities, however interference is an addition of amplitudes so this extinction ratio must be converted to a ratio of amplitudes. The extinction ratio of a commercial available PBS are in the range of $800:1$ [46] the square root of this ratio gives the amplitude ratio, which will be in the order of 3.5%.

The quarter waveplates in the interferometer retard a portion of the light to create a circular polarization, however a QWP has a finite retardance accuracy, for a double pass of the QWP the intensity of the non orthogonally polarized signal with respect to the ortogonally polarized signal can be expressed by equation 6.1 as the minor axis of the polarization ellipse. This ratio can be seen as the extinction ratio of the polarization

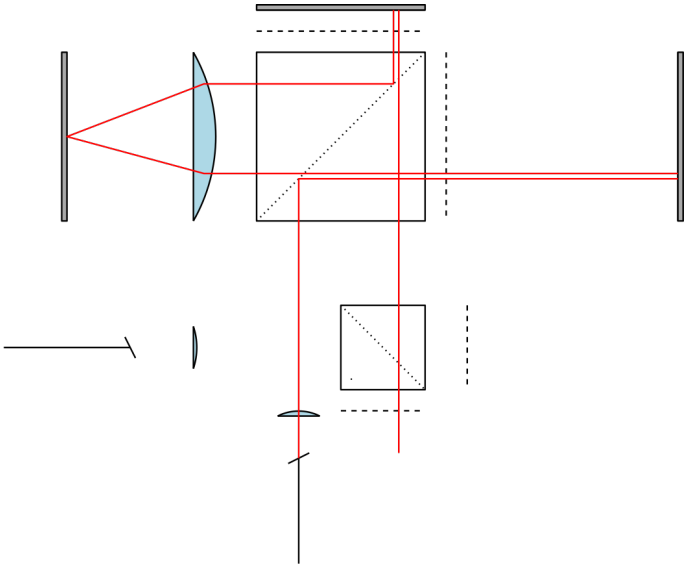

Figure 6.9: The lightpath of the signal where the polarization state is changed in the retroreflector

rotation.

$$B = |E| \sqrt{\frac{1 - \sqrt{1 - \sin^2(2\theta)\sin^2(\beta)}}{2}} \tag{6.1}$$

With the reference frame aligned to the slow axis off the QWP, this gives $\theta = 45°$ and β is the retardance error after two passes of the QWP and $|E|$ is the amplitude of the field. For small retardance errors the desired signal is approximately equal to the Field amplitude, therefore dividing the minor axis by the field amplitude gives the extinction ratio of the polarization rotation. Commercially available quarter waveplates have a retardance accuracy in the order of $\frac{\lambda}{100}$ to $\frac{\lambda}{300}$ [47, 48] For a waveplate with a retardance accuracy of $\frac{\lambda}{100}$ the error signal is 3.1% of the amplitude of desired signal and for a waveplate with a retardance accuracy of $\frac{\lambda}{300}$ the unwanted signal is 1% of the amplitude of the desired signal.

As the error signals that reach the photodetector are products of two subsequent errors giving a ratio of approximately $0.035 * 0.035 = 0.0013$ of the amplitude of the error signal with respect to the desired signal. The magnitude of these errors will be discussed in more detail in section 7.1.2.

Thermal behaviour
Most parts of the concept are thermally stable by design as the measure signal and the first reference signal overlap before separation in PBS2. After separation, the measure signal and the first reference signal overlap with the respective parts of the second reference signal. In the part where the signals are separated in PBS1 and travel to their respective mirrors the signals travel a different direction in a different part of the glass, so this part is sensitive to thermal gradients. However, the distance between the signals is short, so the sensitivity to gradients is also low. The location of the reference mirror determines the location of the virtual thermal reference plane, by choosing an appropriate distance the virtual thermal reference plane can be located such that it is placed at the front mounting surface of the interferometer.

For the cat's eye the parallelism between the incoming beam and the returning beam is dependent on the defocus of the mirror with respect to the lens, if the angle between these beams changes the measured distance changes by a ratio dependent on the angle. For a thermally stable interferometer the change of focal distance of the lens must be corrected for by an appropriate amount of expansion of the distance between the lens and the mirror.

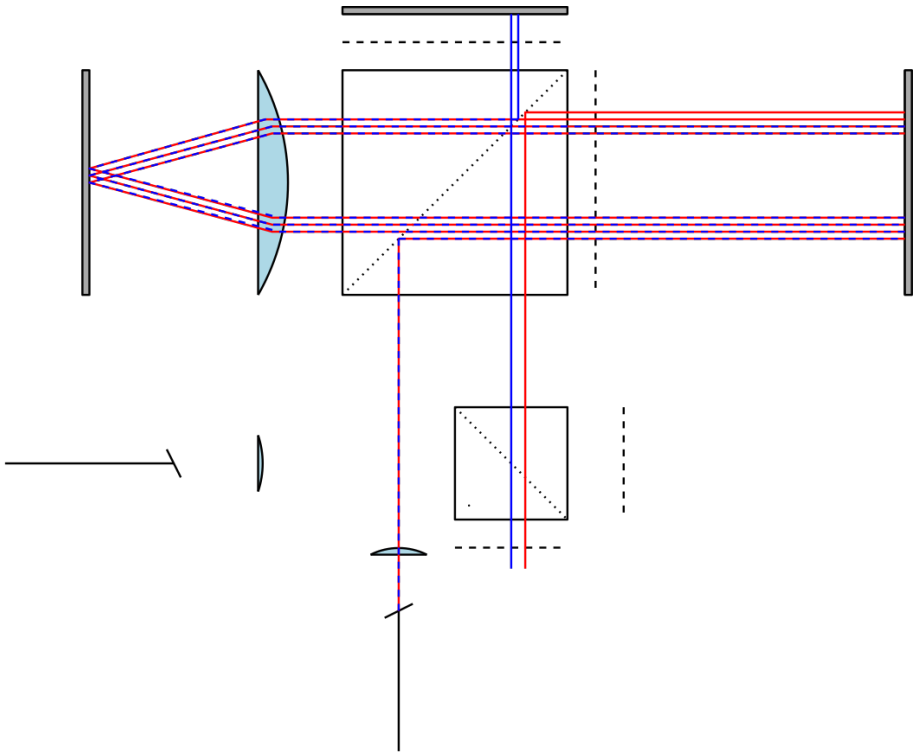

Figure 6.10: The path of the error signal resulting from a non perfect polarization rotation in the last double pass of the QWP, the red line represents the signal where the second error is generated during the subsequent first double pass of the QWP and the blue part is the signal where the second error is generated by the finite extinction ratio during the subsequent second pass of PBS1

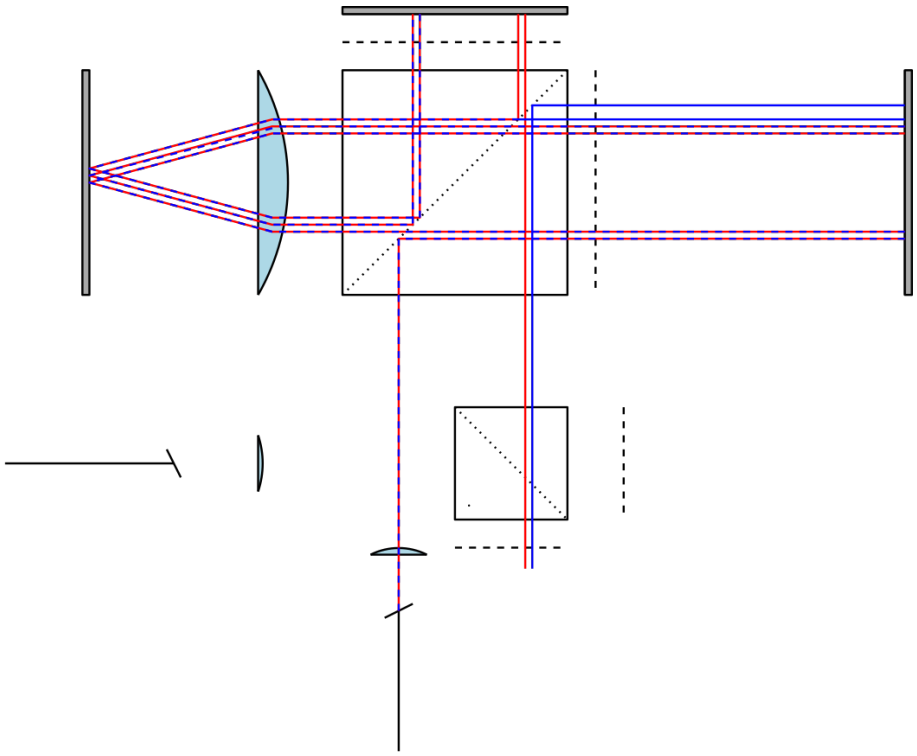

Figure 6.11: The path of the error signal resulting from the finite extinction ratio in the last pass of PBS1, where the red line represents the path of the signal where the second error is generated in the subsequent first double pass of the QWP and the blue line is the path of the signal where the second error is generated by the finite extinction ratio in subsequent fourth pass of PBS1.

6.2.2. Spatially separated HSPMI

Signal path

The signal path of this concept is very similar to that of the concept described in 6.2.1 with a difference that the incoming signals first pass through a polarizing beamsplitter configured in such a way that the resulting beams exit the beamsplitter parallel but spatially separated. Both beams then enter the second polarizing beamsplitter at a different off center location. The measurement beam and the first reference beam have no overlapping path in the interferometer so the signal mixing in PBS2 of concept 1 does not reach any photodetector in this concept. The error signal which would result from a change of polarization state in the retroreflector also does not reach a photodetector directly, but only as a product with the error signal in PBS2 or with the error signal from the spatially separating PBS. Therefore a CCR with metal coating can be used as a retroreflector, however the materials should be chosen such that the cube corner has very good polarization preserving properties such that amplitude of the unwanted polarization state is in the order of a few percent.

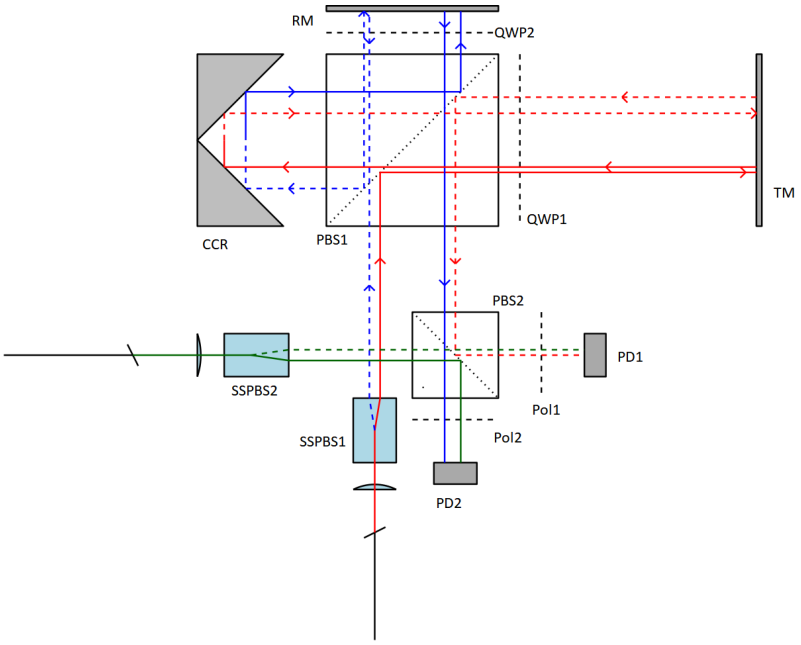

Figure 6.12: The spatially separated variant on the HSPMI, two modified polarizing beamsplitters (SSPBS 1 &2) are used to spatially separate the input signals. A lightbeam travelling behind the drawing plane is indicated as dashed and a lightbeam travelling in front of the drawing plane is indicated as solid.

Error sources

The error signals due to the product of two times a finite extinction ratio or retardance accuracy are still present in this concept however the error signal due to the product of the finite extinction ratio of the PBS1 and the finite retardance accuracy of the QWP do not reach a photodetector. The magnitude of these first mentioned errors is the same as for the first concept.

Thermal behavior

The paths in this concept are not common but spatially separated, this can give a higher sensitivity to thermal gradients in the interferometer. However, for the part of the path where multiple passes through PBS1 are done the signals are symmetric about an axis parallel to the signal path and through the vertex of the CCR reducing the sensitivity to any linear thermal gradients.

6.2.3. Cat's eye beamsplitter concept

In this concept, the retroreflector is used as a beamsplitter and retroreflector as is illustrated in figure 6.6.

Signal path

In order to create a thermally balanced system the first input signal comprising the measurement signal and the first reference signal is separated in a non polarizing beamsplitter configured such that the resulting sig-

nals are traveling parallel to each other while spatially separated. After the separation the signals pass an absorptive polarizer to create a linear polarization state, hereafter the collimated beams enter a first focussing lens at an off-center location which focuses the light onto a reflective linear polarizer. This reflective linear polarizer is configured such that the incident linear polarized light passes. The transmission axis of this polarizer should be a result of the structure of the polarizer itself, for instance, a wire grid polarizer, and not be dependent on the direction of the local p and s polarization such as in a polarizing beamsplitter, as the signals pass through this polarizer with different local p and s directions. After passing through the polarizer the signals pass through a second lens which collimates the light. The collimated linear polarized light passes through a QWP with its fast axis oriented at 45° with respect to the incident linear polarization, making the light circular polarized. A reference mirror is placed in path of the first reference signal whilst the path of the measurement signal passes through a hole in this mirror and is reflected by a second mirror placed in line with the measurement path. The reflection at either the target or reference mirror changes the handedness of the circular polarization. After reflecting of the reference mirror or target mirror the respective beam passes again through the quarter wave plate which changes the polarization to a linear polarization orthogonal to the original linear polarization. The second lens focuses the light onto the reflective polarizer which reflects the signal back through the second lens creating a cat's eye retroreflector. The retroreflected light again passes through the QWP changing the linear polarization to circular polarization. The reflection of the target or reference mirror again changes the handedness of the circular polarization and in the fourth pass through the QWP the light is linear polarized in the same direction as the incident light and passes through the reflective polarizer. Hereafter the light is collimated by the first lens and enters the back of a beamsplitter. The first reference signal enters this beamsplitter at another off center location in the same plane.

The second reference signal passes a different part of the non polarizing beamsplitter, also separating the second reference into two parallel, spatially separated signals. After passing through the linear polarizer both portions of the second reference enter a solid cube corner retroreflector. The last reflective surface of this retroreflector is coated with a beam splitting coating and a right angle prism is placed on the other side of this coating such that the face of the cube corner retroreflector acts as a beamsplitter. In this beamsplitter a first portion of the second reference signal is combined with the measurement signal and a second portion of the second reference is combined with the first reference signal both creating an interference signal. As all signals are linear polarized no additional polarizer is necessary to create interference.

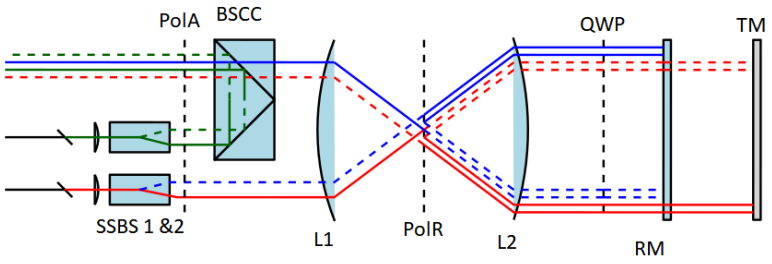

Figure 6.13: Cat's eye beamsplitter concept, two spatially separating non polarizing beamsplitters (SSBS) are used to generate 4 signals of which two travel through the cat's eye beamsplitter consisting of two lenses (L1 and L2) and a reflective polarizer (PolR), and double pass the target distance, after which they combine with the two other signals generating interference.

Error sources

Due to the spatial separation the signals of both interference experiments cannot mix. However, error signals due to imperfect polarization separation and ghost reflections can cause parasitic inference signals. The paths of these signals for an error signal that results of only one imperfection are illustrated in figures 6.14, 6.15 and 6.16.

The first two are the signal paths generated by a reflection of the reflective polarizer of the signal that should pass. An error resulting of only the imperfect retardance accuracy of the QWP does not reach the photodetector but travels back towards the signal input. If the faces of the optical elements are angled slightly this error signal does not reach the photodiode.

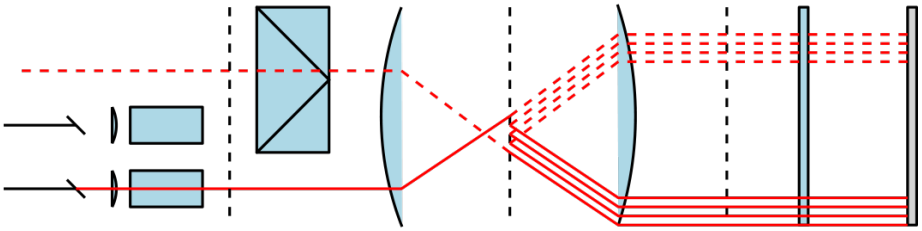

Figure 6.14: The path of the error signal if the signal that should pass through the reflective polarizer at the second pass is reflected.

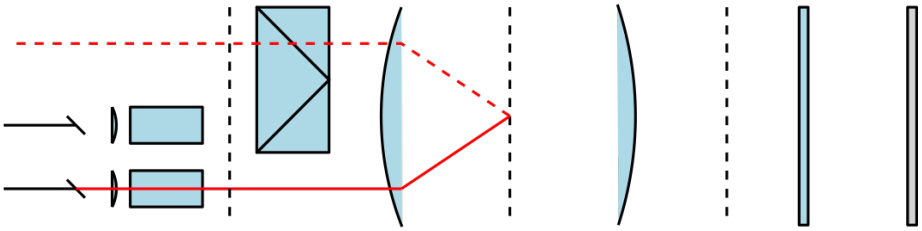

Figure 6.15: The path of the error signal if the signal that should pass through the reflective polarizer at the first pass is reflected.

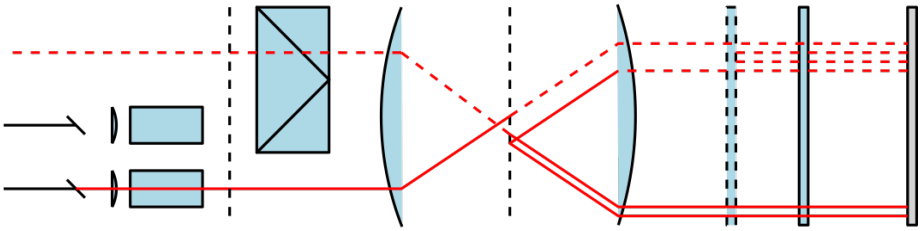

Figure 6.16: The path of the error signal resulting from a ghost reflection of the front surface of the QWP.

Wire grid polarizers can have high extinction ratios for transmission, however, the extinction ratio for reflectance is often lower. For instance, the Versalight wire grid polarizer has an extinction ratio of 2000 : 1 for the transmitted signal intensity but only 80 : 1 for the reflected signal intensity. In this concept the error signals arise from the finite extinction ratio for the reflected polarization, thus these error signals can be of significant magnitude.

Thermal behaviour

Both the measurement signal and the first reference signal travel the same path length, through the same optical components at a different location. For uniform temperature changes, the optical path difference does not change. However as is the case with the cat's eye retroreflector in the first concept the focal length of both lenses changes as a function of temperature, so the mounting of these lenses should be made such that the thermal expansion of the material matches the thermal change of the focal length.

6.2.4. Cubecorner beamsplitter concept

Signal path

In this concept the incoming signals are separated by a non polarizing beamsplitter similar to the one discussed in 6.2.3. The signals then enter the back off a beamsplitting cube corner (BSCC1) (a solid cube corner with a beamsplitting coating on each reflective surface and a right angle prism cemented to each beamsplitting surface) at a different off center location. A portion of the measure signal is reflected by the beamsplitting coating and directed to a beam dump. The transmitted portion of the reference signal travels to a reference mirror where it is reflected and travels back to BSCC1, in BSCC1 a portion of this signal is reflected three times and travels back to the reference mirror where it is reflected for a second time. The signal that is transmitted by the BSCC now enters the backside of the second cube corner retroreflector (BSCC2) which is also a solid cube corner with a beamsplitting coating at one reflective face. At this beamsplitter coating, the measurement signal is combined with a second reference signal and the first reference signal is combined with a third reference signal at a second location on this coating.

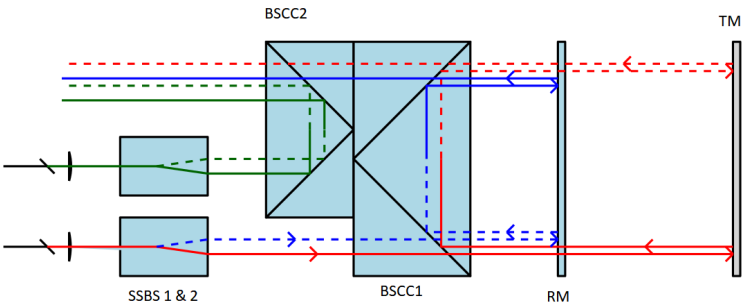

Figure 6.17: A schematic representation of the signals traveling through the concept. The signals that exit the sides of the BSCC are not drawn.

Error sources

In this concept the signals are not separated by polarization but spatially and by intensity, at the coating where the signal is transmitted a part of the signal is reflected as well, a part of this signal travels through the entire cavity twice and is combined with the measurement signal causing errors. If the unwanted signal is attenuated by the BSCC the amplitude of this error signal can be described by equation 6.2 where r_{Bscc} reflectivity of one pass through the beamsplitter.

$$E_{err} = E_{in} r_{Bscc}^3 \tag{6.2}$$

The amplitude of the desired signal can be described by equation 6.3

$$E_{signal} = E_{in} r_{Bscc} \tag{6.3}$$

The transmitted signal is directed back to the light input or towards the sides of the BSCC, where it should be absorbed. If the unwanted signal is attenuated by a filter placed in front of the BSCC the intesity of the unwanted signal is described by equation 6.4 and the measure signal is described by equation 6.5.

$$E_{err} = E_{in} t_{filter}^4 \tag{6.4}$$

$$E_{signal} = E_{in} t_{filter}^8 \tag{6.5}$$

If the unwanted signal is attenuated by the BSCC the ratio between the wanted and unwanted signal is higher than with the use of a filter.

However for this ratio to reach approximately $4 : 1550 * 2\pi$ in amplitude the reflectivity of the BSCC should be lower than 0.12 and the desired signal is then has 1.6% of the intensity of input signals. This would make the sensor very sensitive to stray light.

The error signals resulting from ghost reflections of the outer surface of the BSCC can be minimized by placing these edges at such an angle that the signal resulting from these reflections does not reach a photodetector.

A ghost reflection of the front surface of the BSCC can also be minimized by giving this outer surface a slight tilt, such that the contrast of the interference of this signal with the other signals is very low. For an error signal with a double ghost reflection this wavefront tilt is reversed, but with an AR coating, which can have reflectivities in the order of 0.25% [44] the intensity of a signal that is reflected twice of such an AR coating instead of the target mirror is significantly lower than the main error signal which is a double pass of the cavity.

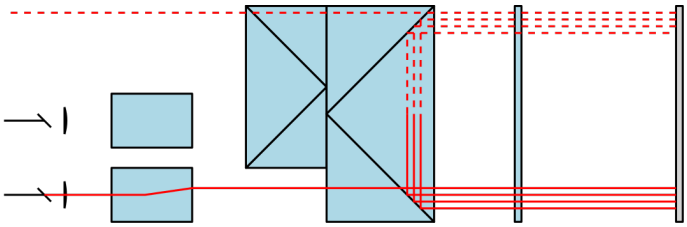

Figure 6.18: The path of the error signal that travels twice through the cavity, in this path the signal is reflected 9 times of a surface of the BSCC.

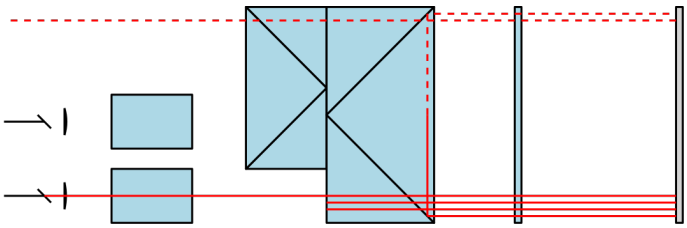

Figure 6.19: The path of a ghost signal of the transmitted light. The interference contrast of this signal can be reduced by making the surface at which the transmitted signals reflect angled with respect to the signal path.

Thermal behaviour

Both signals travel a parallel path through each component and these paths are mirrored around an axis parallel to these beams that goes through the vertex of the BSCC. There are no focussing optics used other than the collimators which may change the focal length due to temperature variations so the concept is entirely insensitive to uniform temperature changes. Since the signals travel parallel through the sensor a thermal gradient from the front towards the back of the sensor has no influence on the difference in optical path.

6.3. Concept selection

The HSPMI inspired concept and the spatially separated variant both have the non correctable errors in the same order of magnitude which is expected to be within specification. The correctable error for the first concept is larger whereas this error is not present in the spatially separated concept.

The cat's eye beamsplitter tube and the cube corner beamsplitter tube are not anticipated to meet the requirement for the maximum non correctable non linear error.

For component availability, the HSPMI inspired concept is more suitable as there is no need for a custom polarizing beamsplitter with a custom coating optimized for angles of incidence smaller than 45° and there is no need for a custom cube corner optimized for polarization preservation.

The thermal drift as a result of the cat's eye retroreflector drifting out of focus poses a more strict requirement on the mechanical mounting of the cat's eye mirror than the use of a cube corner retroreflector, however with a proper choice of materials the required thermal compensation is feasible.

For the alignment aid, all concepts except for the cat's eye beamsplitter concept have the possibility to couple a visible laser to the incoming fiber and use that as a manual rough alignment aid, whereafter the fine alignment can be done with the normal laser by maximizing the signal with a search algorithm. For the cat's eye tube the visible laser will not exit the sensor at the same angle as the infrared laser due to chromatic aberration.

The HSPMI inspired concept is anticipated to meet the requirements best as it meets the performance requirements and also uses the most off-the-shelf components, reducing the lead time.

7

Detailed design Sensor head

The detailed design of the interferometer comprises a detailed optical design, budgeting of the expected errors, tolerancing and an assembly plan. The desired optical performance dictates the optical design and the total allowed error in the error budget. The error budget feeds into the assembly plan as it gives an indication which components might require an active alignment. The assembly plan together with the error budget dictates the mechanical design as it should meet the requirements and provide room for tooling during the assembly and alignment process.

7.1. Optical design

In this section the design of the optics will be discussed. The order works back from the signal pick up toward the delay line as the requirements are defined as properties of the final signal.

7.1.1. Signal pick up

The interference signal needs to be converted to an electric signal for further signal processing. This is done by a photodiode, which is a light-sensitive semiconductor. For the light delivery to the photodiode, there are multiple possible solutions; the photodiode can be placed inside the free-space optical path inside the sensor head, this can be done by focussing the signal on the photodetector, or by placing the photodetector in a collimated signal. The light signal can also be picked up by a fiber to transport the signal from the sensor head towards the control unit. This can be done by either a multimode fiber or a single mode fiber. By using a fiber pick up the sensor head has no internal electronics, dissipating no extra heat to the environment, therefore for a series production interferometer signal pick-up by fiber is preferred. As there are two interference experiments two fibers should be used for signal extraction. As the optical feedthroughs are limited in the vacuum chamber available for qualification the signal pick up is done inside the sensor head and the signals are extracted electrically.

The size of the photodetector should be proportional to the width of the beam to pick up a significant signal, a wider sensor has a bigger surface over which the signal is integrated, resulting in a smaller acceptance for wavefront tilt. As a result, a smaller beam size is preferred to be able to use a smaller detector.

A focusing lens can be placed in front of the photodiode, then a wider beam can be used with a smaller photodetector, however, a wavefront tilt will then shear the focal spots of the interference signals. As the focal spots are very small a small shear will reduce the overlap between the focal spots and thus the interference. In equation 7.1 the waist radius w_0 is approximated for a certain convergence angle θ_{div} where n is the refractive index and λ the wavelength of the light [33].

$$w_0 = \frac{\lambda}{\pi n \theta_{div}} \tag{7.1}$$

The convergence angle can be expressed as the arcsine of the beam radius on the focussing lens divided by the focal distance of the lens.

For a paraxial approximation, the decenter of a focal spot Δ_y due to wavefront tilt θ_{tilt} can be given by equation 7.2 where f is the focal length of the lens.

$$\Delta_y = \frac{\theta_{tilt}}{f} \tag{7.2}$$

The relative beam shear $\frac{\Delta_y}{w_0}$ can be expressed in equation 7.3.

$$\frac{\Delta_y}{w_0} = \frac{\pi n \theta_{tilt} f \arcsin \frac{r}{f}}{\lambda} \tag{7.3}$$

By calculating the loss of interference contrast for this beam shear as is explained in section 7.1.4 it is found that the contrast is reduced to approximately 0.85% for a 100 µrad wavefront tilt, whereas the contrast due to a wavefront tilt for a flat detector is only reduced to 0.98%

Adding focusing lenses also increases system complexity and introduces a sensitivity to the position of the photodiode, as it can move out of focus. Therefore it is chosen to place the photodiodes in the collimated signal.

The size of the beam will be 3.6 mm diameter at the collimator and 4.2 mm diameter at the maximum target distance. This will be discussed in more detail in section 7.1.4.

For this design the selected photodiodes are the FGA 21 supplied by Thorlabs [40] as the rise and fall time are fast enough to follow the signal modulation at 4 Mhz, the active area is big enough to pick up a significant portion of a 4 m beam. The noise equivalent power is 6×10^{-14} WHz$^{-0.5}$ as the system modulates the laser at 4 Mhz but averages the distance information to a 10 Khz displacement output and the power to each photodiode is in the order of 0.2 mW and assuming an interference contrast of approximately 0.5 the noise on the averaged phase measurement is in the order of 1×10^{-7} rad for a wavelength of 1550 nm this results in a sub picometer noise on the displacement. This is well within specification so the noise of the photodiode does not contribute significantly to the total electronic noise of the system.

7.1.2. Polarization optics

Polarizing beamplitters

Extinction ratios are typically defined as a ratio of intensities, however, interference is an addition of amplitudes so this extinction ratio must be converted to a ratio of amplitudes. The laser line polarizing beamsplitters have a high extinction ratio for transmission however the extinction ratio for the reflected light is much lower than that for the broadband polarizing beamsplitters [45, 46]. As the lowest extinction ratio has the greatest influence on the total non linearity error the broadband PBS is preferred for this application.

Quarter waveplates

The quarter waveplates in the interferometer retard a portion of the light to create a circular polarization, however, a QWP has a finite retardance accuracy, for a double pass of the QWP the intensity of the non orthogonally polarized signal with respect to the orthogonally polarized signal can be expressed by equation 6.1 as the minor axis of the polarization ellipse. This ratio can be seen as the extinction ratio of the polarization rotation.

$$B = |E| \sqrt{\frac{1 - \sqrt{1 - \sin^2(2\theta)\sin^2(\beta)}}{2}} \tag{7.4}$$

With the reference frame aligned to the slow axis of the QWP, this gives $\theta = 45°$ and β is the retardance error after two passes of the QWP and $|E|$ is the amplitude of the field. For small retardance errors the desired signal is almost equal to the Field amplitude, therefore dividing the minor axis by the field amplitude gives the extinction ratio of the polarization rotation.

For a polymer waveplate with a retardance accuracy of $\frac{\lambda}{100}$ the error signal is 6.3% of the amplitude of the desired signal and for a quartz waveplate with a retardance accuracy of $\frac{\lambda}{300}$ the unwanted signal is 2.1% of the amplitude of the desired signal.

Waveplates are sensitive to the angle of incidence, for a quartz QWP this sensitivity is very significant, reducing the effective retardance for a slightly tilted waveplate, a polymer zero-order waveplate has a much smaller sensitivity [cite thorlabs] however the retardance accuracy for a perfectly aligned QWP is lower. As the manufacturing tolerances are not infinite and a target tilt rotates the returning wavefront a waveplate with a lower sensitivity to tilt is preferred if the lower retardance accuracy still yields low enough non linearity errors.

7.1.3. Retroreflector

For the cat's eye retroreflector, two aspects need to be considered: the focal distance of the lens, which affects the angle of incidence at the mirror, and thus the polarization crosstalk, the curvature of the mirror which affects the location of the perceived retroreflector.

The focal distance of the cat's eye lens together with the spacing between the incoming and outgoing beam dictate the angles of incidence at each surface. The distance between the beams is determined by the size of the off-the-shelf optics and will be approximately 12 mm.

The relationship between any polarization crosstalk and the angle of incidence is determined by the reflection coeffients given in equation 7.5 and 7.6 where where $n_t \sin\theta_t = n_i \sin\theta_i$ can be used to find $n_t \cos\theta_t = \sqrt{\frac{n_t^2}{n_i^2} - \sin^2\theta_i}$.

$$r_p = \frac{n_i \cos\theta_t - n_t \cos\theta_i}{n_i \cos\theta_t + n_t \cos\theta_i} \tag{7.5}$$

$$r_s = \frac{n_i \cos\theta_i - n_t \cos\theta_t}{n_i \cos\theta_i + n_t \cos\theta_t} \tag{7.6}$$

The phase of the reflection coefficients determines the phase shift for each polarization.

If the linear polarization state is not aligned with the local p and s polarization direction of the reflection the original polarization state can be expressed as a linear combination of these two polarization states. If they are not reflected equally by the mirror the linear combination changes and the resulting polarization state can be different. This effect is the most prominent if the incoming linear polarization state is aligned the least with the local polarization states so both s and p components are equally large.

The cat's eye retroreflector will be configured such that the local p and s polarization are aligned with the two linear polarization states, however, this is only the case for the middle of the beam. To reduce the polarization errors for the rest of the beam the mirror material and the angle of incidence is choosen such that the retardance and diattenuation are minimal for any incoming signal.

The signal which travels at the outer radius of the beam at the cat's eye retroreflector has a rotated plane of incidence with respect to the center of the beam. The local p and s plane have the greatest rotation at the outer radius of the beam where the circumference is tangent to a line through the optical axis.

The rotation of the p and s polarization states is given by $\theta_{pl} = \arcsin\frac{r_{beam}}{r_{center}}$ where r_{beam} is the radius of the beam and r_{center} is the position of the beam center with respect to the optical axis of the cat's eye. Due to beam shear for a rotated target the image of the aperture on the detector as seen in the cat's eye displaces at half the total beam shear. As the crosstalk due to the cat's eye retroreflector first travels to the target mirror and after the cat's eye to the reference mirror and vice versa a target mirror tilt displaces the pupil of the detector for one signal and displaces the incoming signal for the other signal, both shears are half that of the total beam shear.

For a 1 mm pupil radius and a 6 mm position of the center of the beam the rotation of the local p and s plane is 9.5°. To determine the polarization error the linear polarization state is mapped on the local p and s plane, then for each component the complex reflection coefficient is determined and the resulting elliptical polarization is computed. The Jones vector of the mapped polarization can be expressed as $E_0 \begin{bmatrix} \cos\theta_{pl} \\ \sin\theta_{pl} \end{bmatrix} e^{i(kz-\omega t)}$ multiplying this with the the reflection coefficients results in $E_0 \begin{bmatrix} |r_p| \cos\theta_{pl} e^{i\angle r_p} \\ |r_s| \sin\theta_{pl} e^{i\angle r_s} \end{bmatrix} e^{i(kz-\omega t)}$ To compute the crosstalk resulting from this polarization change the Jones matrix must be rotated back and then multiplied by the matrix of a linear polarizer which is placed orthogonal to the original polarization state. The rotation

matrix is given by $R(\theta_{pl}) = \begin{bmatrix} \cos\theta_{pl} & \sin\theta_{pl} \\ -\sin\theta_{pl} & \cos\theta_{pl} \end{bmatrix}$ and the matrix of a linear polarizer is given as $M_p = \begin{bmatrix} 0 & 0 \\ 0 & 1 \end{bmatrix}$
The multiplication of these matrices result in the term for the crosstalk signal as expressed in equation 7.7 where r_p and r_s are calculated according to equation 7.5 and 7.6.

$$\frac{E_{err}}{E_0} = 0.5\sin(2\theta_{pl})\left(-\left|r_p\right|e^{i\angle r_p} + \left|r_s\right|e^{i\angle r_s}\right) \tag{7.7}$$

Due to the relative 180° phase shift between the both polarization states this error source can be simplified to $\frac{E_{err}}{E_0} = 0.5\sin(2\theta_{pl})$. The resulting crosstalk can be calculated by computing the integral of the product of the error dependent on the target angle with the signal amplitude of that location. The angle θ_{pl} can be calculated for any location on the entrance surface of the cat's eye bt equation 7.8 where x and y are the respective coordinates in the plane with its origin at the the optical axis.

$$\theta_{pl} = \frac{x}{y} \tag{7.8}$$

For a beam with its center displaced 6 mm and a beam radius of 1.8 mm from the center the error signal is 0.107. This is a significant error source for the non linearity error. For the sheared pupil the error is 0.123 as the nominal signal incident on this detector is also sheared and thus reduced. and for the sheared Gaussian beam the error is 0.106 The effect of this error will be discussed further in section 7.3.2.

Virtual retroreflection plane
"A retroreflector appears to each incident ray as a plane, perpendicular, reflecting and inverting surface." [36] The location of this surface can be chosen by the design of the cat's eye retroreflector, a plane mirror places this inverting surface at one focal distance before the cat's eye lens, a spherical mirror with a radius of curvature that equals the focal distance places this surface at the same location as the cat's eye lens.

In this design a flat mirror is chosen and the reference mirror is mounted at such a distance that it is placed in the retroreflecting plane. As a result, the interferometer is insensitive to a small reference mirror tilt. This is particularly useful for mounting mirrors in the virtual reference plane for qualification and alignment as the signal is also insensitive to a target mirror rotation if this mirror is then placed at the virtual reference plane.

As the space in front of the cat's eye lens is partly glass which refracts the light, the physical distance from the lens to the retroreflection plane needs to be corrected for this interface. The beamsplitter can be modeled as a thick plan plate. The angle of the light beam reduces in the medium with a higher refractive index, following snell's law and the small angles approximation the angle is inverse proportional with the refractive index following equation 7.9 where θ_i is the angle inside the medium and θ_o is the angle outside the medium with the higher refractive index.

$$\theta_i = \frac{n_1}{n_2}\theta_o \tag{7.9}$$

The distance to the perceived retroreflector scales with the same relation, so by placing the PBS in front of the cat's eye retroreflector the retroreflecting plane moves further away from the cat's eye.

For a 46 mm focal distance for the cat's eye lens with 25.4 mm glass cube in front with a refractive index of 1.68 there is an 30 mm of path left before the virtual retroreflecting plane to create some space for mounting of these components and to place the QWP.

7.1.4. Beam size

To determine the beam size the factors dependent on the beam size are first discussed, and then the collimation of the light is discussed to determine what optics are necessary to create the required beam size.

Beam shear
A rotating target causes beam shear in the returning signal, the beam shear can be expressed as a function of the target distance and the target rotation as given in equation 7.10 for small angles.

$$BS = 4 * L_{target} * \theta_{target} \tag{7.10}$$

Where BS is the beam shear in mm L_{target} the target distance in mm and θ_{target} is the rotation of the target mirror in radian. The interference signal is only generated in the part where the reference beam and the target

beam overlap. For the specified target rotation at the preferred distance, the resulting beam shear is $0.8mm$.

The intensity of the interference signal is given by the last term in equation 7.11 where E_1 is the amplitude of the first field and E_2 is the amplitude of the second field and ϕ is the phase between the fields.

$$I = E_1^2 + E_2^2 + 2E_1E_2cos(\phi) \tag{7.11}$$

The Intensity of the interference signal between two sheared gaussian distributed fields can be described by equation 7.22 where A is the sensor area, w is the e^{-2} radius of the beam and BS is the beam shear and E_1 is given by equation 7.13 and E_2 is given by equation 7.14.

$$I_{interference} = \iint_A E_1(x,y)E_2(x,y)dA \tag{7.12}$$

$$E_1(x,y) = e^{\left(\frac{-(x^2+y^2)}{w^2}\right)} \tag{7.13}$$

$$E_2(x,y) = e^{\left(\frac{-((x+BS)^2+y^2)}{w^2}\right)} \tag{7.14}$$

Not only the intensity of the interference term reduces due to beam shear, the DC intensity also reduces as there is less light reaching the detector. As a result, the contrast of the interference reduces slower than the interference intensity. The normalized interference contrast can be described by equation 7.15.

$$C = \iint_A \frac{E_1(x,y)E_2(x,y)}{E_1(x,y)^2 + E_2(x,y)^2}dA \tag{7.15}$$

As a gaussian beam diverges after passing the waist the collimated beam expands with an increasing target distance, as a result the second reference signal has a smaller diameter than the measure signal for a non zero target distance. The local beam radius van be calculated by equation 7.16 where $w(z)$ is the beam radius where the intensity drops to e^{-2}, w_0 the waist radius, z_r the rayleigh range which can be calculated by equation 7.17 and z is the distance from the waist.

$$w(z) = w_0\sqrt{1 + \left(\frac{z}{z_r}\right)^2} \tag{7.16}$$

$$z_r = \frac{\pi w_0^2 n}{\lambda} \tag{7.17}$$

The relation for a beam diameter at 4 m and the waist diameter at the collimator is shown in figure 7.1 The beam radius is chosen such that it is placed located at the right side of this minimum as the beam size and divergence are both minimal.

For a beam with a 1.8 mm waist radius at the collimator the beam radius after four meters of travel has expanded to 2.1 mm radius.

In figure 7.2 and 7.3 the contrast and interference intensity integrated for a 1.8 mm first beam e^{-2} radius over a 2 mm diameter photodiode are plotted against the e^{-2} radius of the second beam. It is seen that the contrast does not decrease significantly but the interference intensity decreases with 11% over the maximum operating range of the sensor.

7.1.5. Collimation of the light

For the collimation of the light emitted by fibers a collimating lens is used, the fiber end is placed at the focal point of the lens to create a collimated beam of light. The focal distance off the lens determines the beamdiameter. Equation 7.16 can be used to determine the size of the beam at any distance away from the fiber if the waist radius is taken to be the half of the mode field diameter exiting the fiber. However, due to to the short rayleigh range the location of the collimator will in the far field, thus equation 7.1 can be used to determine the divergence angle of the light beam exiting the fiber. For a 1.8 mm beam radius the focal length of the lens is 18.75 mm. For the demonstrator a fixed focus collimation package is used as they are off the shelf available [49].

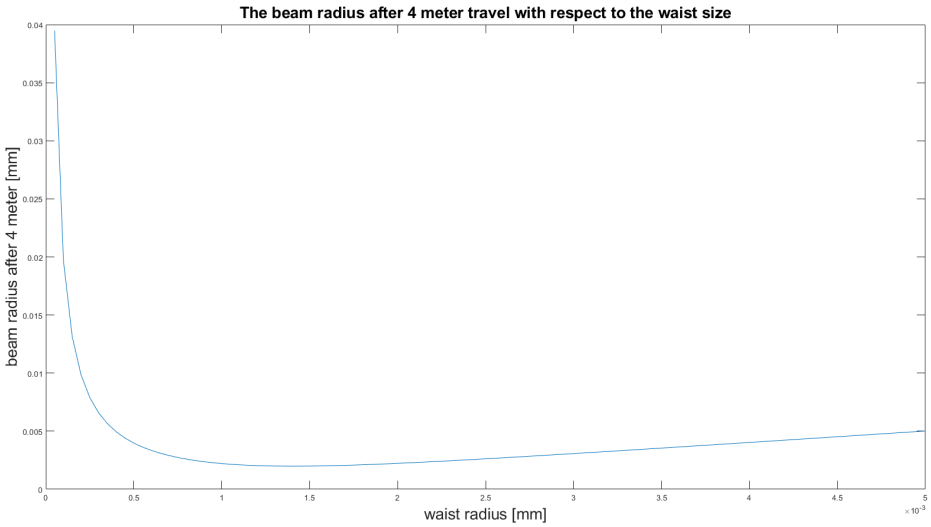

Figure 7.1: The beam size after 4 meters travel with respect to the waist radius, it can be seen that the the beam diameter at 4 m is has a minimum from from a waist size of 1 mm to 2 mm.

7.1.6. Delay line

Polarization control
In the sensor head the measure signal and first reference signal are separated by polarization state, to create an approximate equal signal for both measurements the polarization state is preferably a linear polarization state with an 45° angle with respect to the p and s polarization of the first PBS or a circular polarization state. As the polarization state only determines the intensity of the input signal the exact polarization state is not critical.

The laser source is a DFB laser that emits a linear polarization state [52]. The requirement for some polarization control can be achieved with a standard PM fiber [42].

Optical path difference
For a 1 m target distance, the difference between the minimal path length difference and the maximum path length difference is 4 m for the double pass sensor head. For minimal 90% signal intensity for both signals the modulation depth must be within 1.180 and 1.533 rad.

To satisfy the minimum zero difference and the maximum at 4 meter difference the optical path difference in the delay line must be 13.7 m. For a PM fiber with a refractive index of approximately 1.4 a fiber length difference of 10 m satisfies these requirements.

As the OPL is increased by a factor $\frac{18}{1}$ the laser modulation is decreased by the same factor. If the gas pressure in the reference cell can be adjusted such that the width of the absorption peaks is decreased by the same ratio the measured absorption signal does not change and the wavelength control of the laser remains effective. The absorption width scales with the pressure inside the gas cell by the pressure broadening coefficient, this relationship can be approximated as linear for low pressures [39]. the width of the absorption peak can be scaled to $\frac{1}{18}$ of that of a 25 Torr gas cell by decreasing the pressure to approximately 1,4 Torr. Such a gas cell is possible [54].

7.1.7. Signal folding

Both signals enter the sensor head via an optical fiber, it is advantageous to position the fiber input such that the fibers oriented in the same direction as the fiber can then be placed next to each other. To create this fiber arrangement an extra folding flat should be introduced in the interferometer. For stability, a glass prism is used which is cemented against the PBS. This prism is also used as a glass spacer between PBS1 and PBS2. The orientation of this prism can change during the curing of the cement, but after curing the orientation of the mirror plane and both polarizing beamsplitters are fixed with respect to each other.

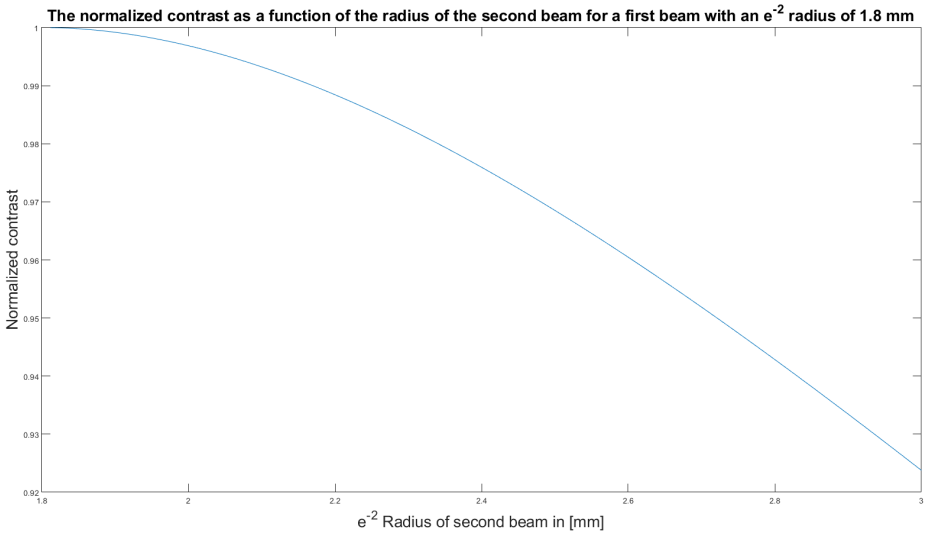

Figure 7.2: The interference contrast for an expansion of the target beam, it is illustrated that the contrast does not decrease significantly over the expansion of the beam

7.2. Error budgets

There are multiple error budgets for the sensor head. There is an error budget for the thermal instability, there is a budget for the contrast of the interference signal which is affected by the wavefront error, wavefront tilt and beam displacement. Non linearity errors due to signal mixing are budgeted in a separate budget. The linear error due to a non parallelism between the retroreflected signals is discussed separately as this is the only linear error present in the sensor head.

7.3. Linear errors

If the interferometer does not measure perpendicular to the mirror a cosine error is introduced. As the alignment of the interferometer with respect to the plane mirror is part of the use case the error due to a misaligned interferometer is not budgeted here. However, is the cat's eye retroreflector is not aligned perfectly the returning signal is not parallel with the incoming signal creating a cosine error even if the target mirror is perfectly aligned. Only half of the measurement signal is misaligned, so the error is minimal if the target mirror is tilted such that the angular error is divided over both passes of the target distance, the error can then be described by equation 7.3 where the relation between the angle θ_{cos} and the defocus is given by equation 7.19 where y is the radial spot location and d_z is the defocus of the mirror.

$$e_{cosine} = L_{target}(1 - \cos(\theta_{cos}/2)) \tag{7.18}$$

$$\theta_{cos} = \frac{2d_z y}{f^2} \tag{7.19}$$

If the angular error between the signals of the cat's eye is then 100 µrad the resulting linear error is 0.625 nm for the required target distance of 0.5 m and 1.25 nm for the extended target distance of 1 m.

7.3.1. Contrast budget

The contrast of the interference signal is influenced by multiple factors such as wavefront errors, beam shear and beam rotation. These influences on the contrast are budgeted in the contrast budget.

Wavefront errors

The optics through which the signal passes can distort the wavefront locally due to surface roughness. The interference with this distorted wavefront is integrated over the photodiode, if the distortion is significant

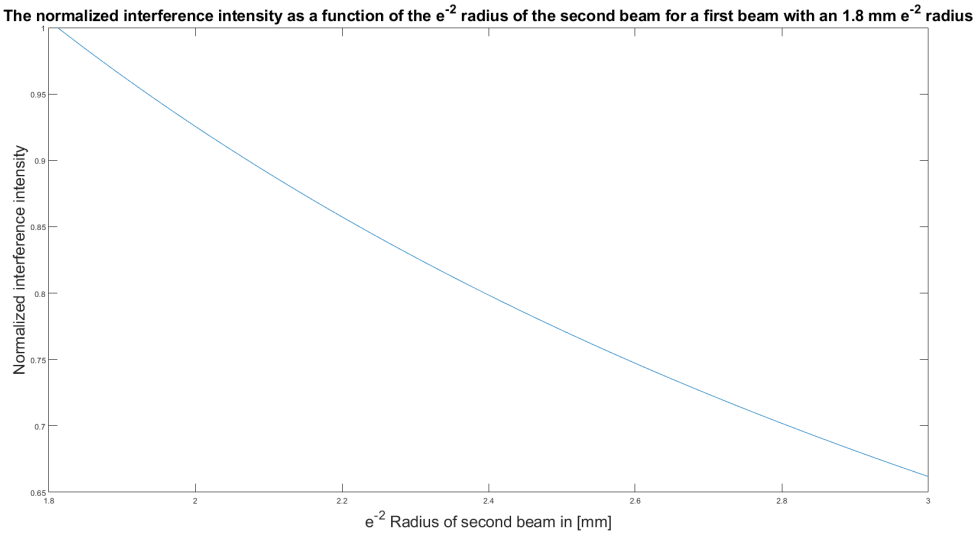

Figure 7.3: The interference intensity for an expansion of the target beam, it is illustrated that the intensity does decrease significantly over the expansion of the beam, this reduces the signal to noise ratio of the interferometer. For an expansion from an 1.8 mm to an 2.1 mm e^{-2} radius the interfernece intensity decreases with a factor 0.89.

Error source	magnitude of effect	Effect on contrast
Wavefront tilt	200 µ	0.92
Wavefront overlap	0.8 mm	0.91
Wavefront error	180 nm	0.75
Signal unbalance	0.8	0.98
Modulation depth	1.180-1.533 rad	0.9
Total contrast		0.61

Table 7.1: The contrast budget comprising the effects which influence the interference contrast and the magnitude of these effects.

with respect to the wavelength the average interference intensity reduces. By assuming a uniform distribution from $-h_{surf}$ to h_{surf} where $h_{surf} = RMS$ the ratio between the intensity of the peak of the disturbed interference and a nominal signal can be described by equation 7.20. This gives an estimate of the contrast reduction.

$$\frac{1}{2h_{surf}} \int_{-h_{surf}}^{h_{surf}} cos\left(\frac{2\pi x}{1550}\right) dx \tag{7.20}$$

If the roughness is assumed to be normal distributed the contrast reduction can be calculated by equation 7.21

$$\frac{1}{RMS * \sqrt{2\pi}} \int_{-\infty}^{\infty} e^{-\frac{1}{2}\left(\frac{x}{RMS}\right)} cos\left(\frac{2\pi x}{1550}\right) dx \tag{7.21}$$

The P-V errors are approximated to RMS errors by dividing the P-V value by a factor $4,5$ for a combination of random errors and low order aberrations, this is more conservative than only random errors which can be approximated by dividing by a factor 5 [34].

The approximation as a normal distribution reduces the contrast to $76,9\%$ for a 179 nm surface error and the uniform distribution reduces the contrast to $75,7\%$ for the same surface roughness.

Wavefront overlap
Interference only takes place if the wavefronts overlap, as the beams have an approximate gaussian profile a shear between the interfering beams can affect the intensity of the interference and thus the contrast. Positional tolerances and beams shear due to a target rotation are the biggest influences for the wavefront overlap. The contrast of the interference signal is determined by the intensity of the interference signal over

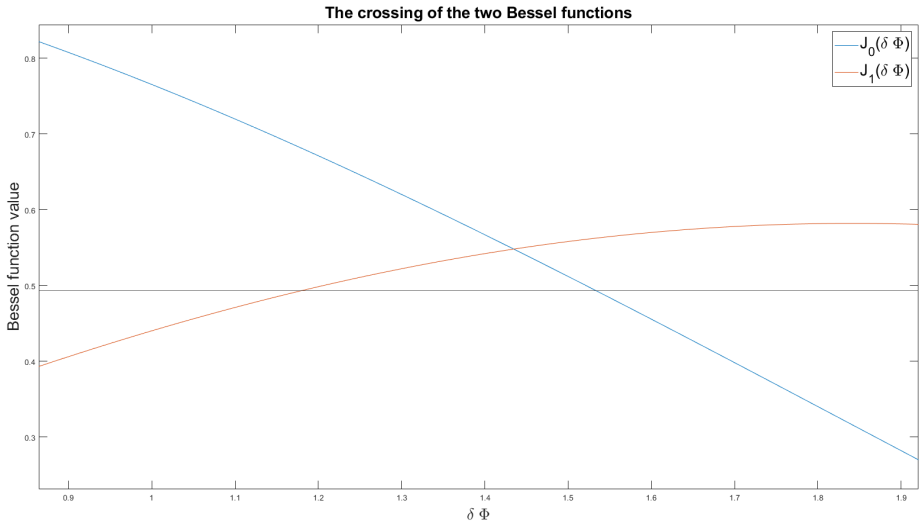

Figure 7.4: The J_0 and J_1 Bessel function and a line representing the value of 90 % of the crossing value

Error source	Surface error RMS [nm]	Amount of interactions	Sensitivity	Resulting error [nm]
Entrance surface glass spacer	35	1	0.683	24
Folding mirror	35	1	2	70
Spacer glass-glue	35	3	0.142	9
PBS1 glue-glass interface	35	2	0.142	35
PBS1 reflection	35	2	2	99
PBS1 glass-air interface	35	6	0.6832	59
Cat's eye mirror	14	1	2	28
Cat's eye lens	34	4	0.683	47
Target mirror	14	2	2	40
PBS2 glue-glass interface	35	1	0.142	5
PBS2 reflection	35	1	2	70
PBS2 glass-air	35	3	0.683	24
QWP glass-air	35	4	0.683	48
Polarizer	35	2	0.501	25
RSS error				179

Table 7.2: Tolerance budget for short spatial errors, the sensitivity is the effect of one interaction of the surface with the wavefront.

DC intensity. The amplitude of the interference signal between two sheared gaussian distributed fields can be described by equation 7.22 where A is the sensor area, w is the e^{-2} diameter of the beam and BS is the beam shear.

$$I_{max} \iint_A e^{\left(\frac{-(x^2+y^2)}{w^2}\right)} e^{\left(\frac{-((x+BS)^2+y^2)}{w^2}\right)} dA \tag{7.22}$$

In figure 7.5 and 7.6 the relation between the interference contrast and intensity and the beam shear is illustrated for a 2 mm diameter detector.

To create a maximum signal contrast the collimators are aligned such that the manufacturing tolerances do not create beam shear, but only a rotation of the target mirror introduces beam shear. To determine the range needed for the collimator alignment the manufacturing tolerances and respective sensitivities are budgeted in table 7.3. This budget is valid for the target signal and the reference signal as the target mirror is assumed to be placed orthogonal to the exiting signal, thus the target distance does not introduce an extra beam shear. The reference mirror is not necessarily orthogonal to the signal as it is placed in the virtual retroreflection

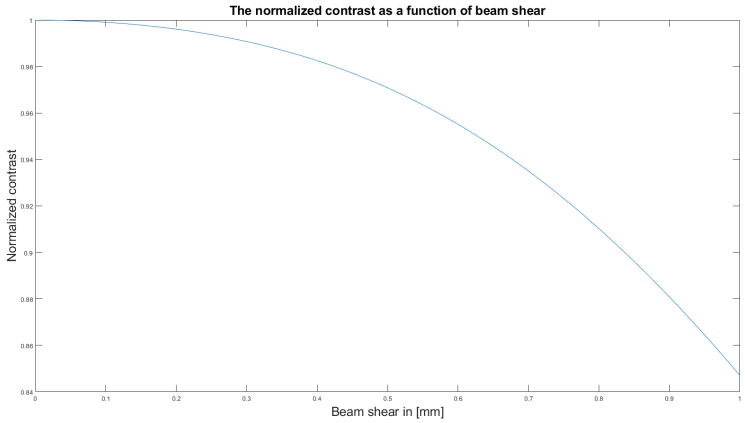

Figure 7.5: The normalized interference contrast with respect to the beam shear, integrated over a 2 mm diameter photodiode with a 3.6 mm diameter not sheared beam and a 4 mm diameter sheared beam.

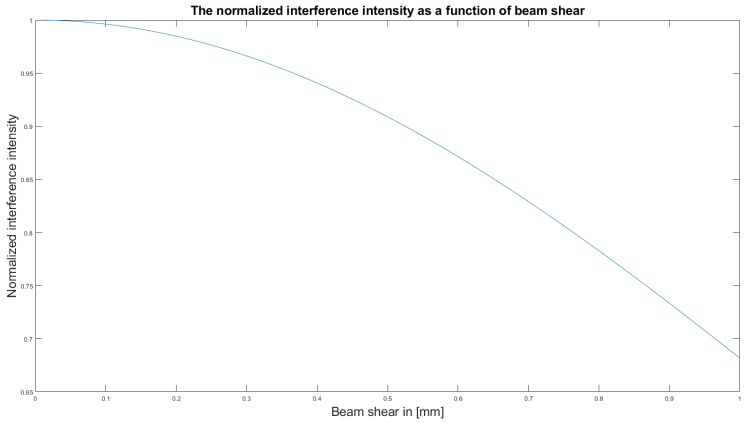

Figure 7.6: The normalized interference intensity with respect to the beam shear, integrated over a 2 mm diameter photodiode with a 3.6 mm diameter not sheared beam and a 4 mm diameter sheared beam.

plane.

Wavefront rotation

A wavefront tilt of one wavefront with respect to the other wavefront results in a phase difference over the active area of the photodiode. If the phase difference is in the order of the π rad a dark and a bright fringe will lie on the photodiode and the observed interference contrast is greatly reduced. Assuming a flat wavefront the relation between the interference contrast observed on the photodiode and the tilt of the wavefront can be described by equation 7.23.

$$\iint_A E_1 E_2 cos\left(\frac{2\pi\alpha}{\lambda}\right) dA \tag{7.23}$$

With an alignment step, the wavefront tilt due to manufacturing tolerances is removed. In table 7.4 the sensitivity analysis is shown dictating the range of the alignment. The resulting wavefront tilt is the result of the finite alignment precision and the thermal expansion of the cat's eye defocus. If the alignment is done to 100 µrad precision another 100 µrad can be budgeted for the defocus due to imperfect thermal expansion.

The contributions of the other errors resulting in a wavefront tilt are much smaller than the error due the rotation of the mirror surface of PBS2,

Error source	Sensitivity First order	Tolerance	Resulting error
Rotation glass assembly	0.097 mm/mrad	2 mrad	0.2 mm
Rotation fold mirror for	0.29 mm/mrad	1 mrad	0.3 mm
Translation fold mirror	1	0.1 mm	0.1 mm
Rotation PBS1	0.098 mm mrad	3 mrad	0.3 mm
Translation PBS1	2	1 mm	0.2 mm
Cat's eye lens decenter	2	1 mm	0.2 mm
PBS2 translation	1	0.1 mm	0.1 mm
Linear addition total			1.4 mm
RSS total			0.64 mm

Table 7.3: Tolerance budget for beam shear of the target signal before the alignment of the collimators with respect to each other. The target is assumed to be placed orthogonal to the first incident light beam. The second signal is assumed to be aligned such that both wavefronts are parallel for the common path towards the photodetector as would be the case during alignment. The lengths used to compute these sensitivities are as follows L_{sp1} = 19.05 mm is the length of the first glass spacer from the entrance of the glass assembly to the folding mirror, L_{fm} = 16.35 mm is the length of the path from the folding surface to PBS1, L_{PBS1} = 25.4 mm is the length of PBS1 L_{PBS-VR} = 23.95 mm is the distance from PBS1 to the virtual retroreflection plane, L_{PBS2} = 25.4 mm is the length of PBS2 and L_{sp2} = 29.9 mm is the length of the spacer between PBS1 and PBS2. These sensitivities are checked by a zemax sensitivity analysis.

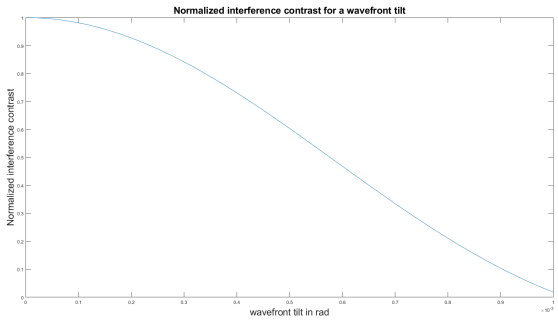

Figure 7.7: The Normalized interference contrast for a wavefront tilt for a 2 mm diameter detector for a 4 mm beam diameter

Signal unbalance
The contrast between two interfering signals can be written as equation 7.24.

$$C = \frac{2E_1E_2}{E_1^2 + E_2^2} \tag{7.24}$$

For a signal reduction of 80% for one signal the contrast is still 97.5% of the maximum contrast. The relation between the alignment of a linear polarizer and the signal strength for a polarizer placed at 45° is given in equation 7.25.

$$\frac{E}{E_0} = \frac{\cos 45° + \theta_{pol}}{0.5\sqrt{2}} \tag{7.25}$$

This results in an alignment of the polarizers to 0.18 rad, manufacturing tolerances are assumed to be much better than this specification, therefore no addition tolerances need to be added.

7.3.2. Non linearity errors

Parasitic Interference Signals (PIS) from for example ghost reflections and imperfect polarization optics can cause deviations from the linearity of the interferometer output.

The resulting intensity of four signals mixing can be described by equation 7.26 where E_n with $n = 1,2,3,4$ is the respective field amplitude and $\phi_{n,m}$ the phase difference between field n and m.

$$I = E_1^2+E_2^2+E_3^2+E_4^2+2\left(E_1E_2\cos\phi_{1,2} + E_1E_3\cos\phi_{1,3} + E_1E_2\cos\phi_{1,3} + E_2E_3\cos\phi_{2,3} + E_2E_4\cos\phi_{2,4} + E_3E_4\cos\phi_{3,4}\right) \tag{7.26}$$

Error source	Sensitivity First order	Tolerance	Resulting error
Right angle prism angular tolerance	2	1 mrad	2 mrad
Entrance - exit surface parallelism	0.68	3 mrad	2.4 mrad
Cat's eye defocus	5.6 mrad/mm	18 µm	100 µrad
PBS2 rotation	3.36	3 mrad	10.1 mrad
Linear added error			14.2 mrad
RSS error			10.5 mrad

Table 7.4: Error budget for relative wavefront tilt before the alignment of the collimators with respect to each other. The greatest error source is the tolerance on the rotation of PBS2, dictating the stroke of the alignment tool.

Assuming the E_1 and E_2 to be the amplitude of the desired fields the field with n = 3 and 4 can be sources of errors. The quadratic term is a constant offset, only the cross terms can result in an error in phase determination.

The non linearity error in radians due to a single mixing term can be described by equation 7.27 if the ellipse fitting has not corrected for any deviation.

$$e_{mix,3,1} = \arctan \frac{\sin\phi_{1,2} + \frac{E_3}{E_1}\sin\phi_{1,3}}{\cos\phi_{1,2} + \frac{E_3}{E_1}\cos\phi_{1,3}} - \arctan \frac{\sin\phi_{1,2}}{\cos\phi_{1,2}} \tag{7.27}$$

For very small errors which are90° out of phase with the desired signal this error is maximal and the equation reduces to equation 7.28.

$$e_{mix,3,1} = \frac{E_3}{E_1} \tag{7.28}$$

With three signals present, there is a second cross term resulting in a second deviation from linearity, however, the modulation depth of one of these cross terms is very low as these signals have both traveled through either the delay line or the reference line. This cross term only contains the DC quadrature signal as the modulated quadrature signal approaches zero. The DC component however is greater as the J_0 Bessel function is maximal at zero modulation depth. The signal amplitude of this error is than $\frac{1}{J_0(\Phi_{cros})} = 1.825$ where $J_0(\Phi_{cros})$ is the value of the crossing of the zeroth and first Bessel function of the first kind. The phase of this second cross term is dependent on the phase of the desired signal and the first crossterm following equation 7.29 where $\phi_{n,m}$ is the phase difference between signal n and m.

$$\phi_{1,3} - \phi_{1,2} = \phi_{2,3} \tag{7.29}$$

If the error due to mixing between signals 1 and 3 is maximal, they are orthogonal to each other, resulting in $\phi_{2,3} = \pm 90°$. The DC quadrature term for a signal with a 90° phase is zero, so if one error is maximal, the error due to the second cross term is zero, therefore these errors do not add linear but can be added quadratically. As the term with little modulation depth has an extra scaling factor the total error due to a parasitic interference signal can be described by equation 7.30 assuming $E_1 = E_2$.

$$e_{mix,3} = \sqrt{e_{mix,3,1}^2 + e_{mix,3,2}^2} = \frac{E_3}{E_1}\sqrt{1 + 1.825} = 1.68 * \frac{E_3}{E_1} \tag{7.30}$$

Some of these errors can be compensated, such as error signals with constant phase difference which are compensated by ellipse fitting, or an error signal with a known phase difference and a known magnitude can be corrected for as the signal can be subtracted from the measured signal. The magnitude of this signal can be established by a calibration step. However, error signals with a non constant phase difference are harder to correct for without further knowledge. For interference signals with a non constant phase of which the phase is not known the interference intensity should be so small that the Root sum square addition of all the errors does not cause a phase error greater than $\frac{4nm}{1550nm} * 2\pi = 0.016$ rad.

Static parasitic interference signals
The amplitude of the desired signals is significantly greater than that of the unwanted signals as a result of the design effort, the cross term of an error signal with the desired signal is the greatest error source. However, if the phase difference is approximately constant and the modulation of that phase is negligible or approximately equal to the modulation of the desired interference term these terms also reduce to an offset in the signal. For a double reflection between two parallel surfaces inside the interferometer the phase difference is almost constant, as it only changes with temperature and the distances inside the interferometer are in the order of 10^{-2} m with an thermal expansion in the order of $10^{-5}\,K^{-1}$ giving a temperature dependent displacement in the order of 0.1 µm/K resulting in a phase difference 0.4 rad/K for the parasitic interference. If the temperature changes the measured distance also changes as both of the interference experiments are unbalanced.As the phase sensitivity to temperature of the PM fibers is in the order of $5 \times 10^{-6}\,K^{-1}$ [37] with a fiber length of multiple meters the displacements in each of the interference experiments are assumed to be significantly greater than the change of phase for the static PIS the ellipse-fitting correction can correct for these errors.

Known errors
The signal mixing due to a finite extinction ratio in PBS2 causes a significant non linearity error as the magnitude of this signal is significant, however the phase difference of this mixing signal with the reference signal is known from the other interference experiment. If the magnitude of this crosstalk is established by a calibration step this error can be corrected for. The stability of the magnitude of the error between calibration steps should be in the same order of magnitude as the uncorrected non linearity errors.

Cat's eye retroreflector error
The error signal due to the polarization change in the cat's eye retroreflector reflects of both the target mirror and the reference mirror once. By placing the reference mirror at such an angle that these reflections introduce a wavefront tilt the interference contrast of this can be reduced by the same factor as shown in figure 7.7. If the reference mirror is rotated by at least0.9 m and the target mirror is tilted 0.4 m which is greater than the requirement for angle acceptance, the wavefront rotation is 1 m reducing the interference contrast of this error signal by a factor of 0.018. As the reference mirror is placed at the virtual retroreflecting plane no beam shear will occur. The resulting error due to this crosstalk source is then$0.013 * 0.018 = 0.0024$.

Two times the QWP
The error due to two times a retardance error is an extra double pass of the measured cavity. For a perfectly aligned target any effects that would reduce the interference contrast of this error will also reduce the contrast of the desired signal. For a tilted target the beam shear for the error signal is twice that of the measurement signal, which reduces the intensity of this error for a tilted target at a longer target distance. For the internal measurement this effect is negligible as the reference mirror is mounted in the virtual retroreflector plane. As calculated in section 7.1.2 the magnitude of this error is $0.063^2 = 0.0040$.

QWP and PBS1
The error due to the finite extinction ratio of PBS1 and the QWP can either be due to the finite extinction ratio for transmission or for reflection. They are 1 : 402 and 1 : 955 respectively. Which translate to a 5.0% and a3.2% amplitude. In all the possible paths this signal takes it always reflects an odd amount of times of the target and reference mirror. The same effect used for the crosstalk due to the cat's eye retroreflector can be used to reduce the interference contrast for this signal. The magnitude of this error for the extinction ratio for transmission is then $0.063 * 0.05 * 0.018 = 0.000057$ For the extinction ratio for reflection the magnitude of this error is $0.063 * 0.032 * 0.018 = 0.000036$.

Two times PBS1
An error due to the product of two times the finite extinction ratio of PBS which is a combination of the extinction ratio for transmission and reflection. Also reflect an odd amount of times of each mirror, so the same wavefront tilt can be used to reduce the interference contrast again. The magnitude of these errors is then $0.032 * 0.05 * 0.018 = 0.000029$

However in the last pass of the PBS the error signal due to a finite extinction ratio for transmission as a product with the same finite extinction ratio mixes this signal with the incoming signal, creating a second double pass of the target distance, and the same happens for the finite extinction ratio for reflection for the first reference

signal. For one signal the error signal is then the product of two times the extinction ratio so $0.05 * 0.05 = 0.0025$ for the target measurement and $0.032 * 0.032 = 0.0010$ for the reference signal.

The path length of this error signal is always longer than the measure signal, therefore the modulation depth of this error is greater. For a greater modulation depth than the desired signal the demodulated quadrature signal is greater than the DC quadrature signal in comparison to the desired signal. If the phase of this parasitic interference signal is 0.5π or 1.5π The amplitude of the demodulated quadrature signal is maximal, which will produce the greatest non linear errors for the signal mixing term with modulation depth. The maximum modulation depth of this error source is the modulation depth of the delay line with twice the possible variation in modulation depth added. For a maximum target distance this difference in modulation depth is at a maximum, the modulation depth for the desired signal is then 1.533 rad giving a $J_1(\Phi) = 0.5623$ and the modulation depth of the error signal is then 1.886 rad giving a $J_1(\Phi) = 0.5815$. The non linearity error scales with the same factor which is approximately 1.034. This is not a significant increase in error, and the DC signal mixing error still is significantly greater.

Combined uncorrected errors
The addition of the non linearity errors which can not be corrected directly is shown in table 7.5 it follows that the non linearity error of the interferometer is 0.73 nm.

Name of error	amount of different paths	relative signal amplitude	phase error
Retroreflector error	2	0.0023	0.0056
2x QWP	2	0.0040	0.0094
PBS1,t & QWP	3	0.000057	0.000165
PBS1,r & QWP	3	0.000036	0.000086
PBS1,t & PBS,r	4	0.000028	0.000097
2x PBS1,t	1	0.0025	0.0042
2x PBS1,r	1	0.001	0.0017
Total error RSS			0.0119

Table 7.5: The sources of uncompensated non linearity errors, the magnitude of the error signals and the resulting non linearity errors. The total phase error of 0.0119 results in a 2.92 nm non linearity error for the optical path length. As the double pass sensor head has a factor four optical resolution this results in a 0.73 nm non linearity error.

7.3.3. Thermal drift

Thermal drift of the signal is the result of any thermal influence on the measurement signal, for instance the thermal expansion of unbalanced portions of the signal, but also a cosine error due to a defocus of the cat's eye retroreflector due to a mismatch in the thermal balancing.

Unbalanced thermal expansion
The sensor head is thermally balanced by concept, however due to finite manufacturing precision in the non common paths unbalanced thermal expansion can be measured. The sensitivity for these parts is computed as the expansion of the glass part times the difference in refractive index with the environment and the change of refractive index as a product with the length of the unbalanced part. This can be described by equation 7.31 where n is the refractive index of the medium, α the Coefficient of Thermal Expansion (CTE), $\frac{dn}{dT}$ the thermo-optic coefficient and L is the length of the path through the medium.

$$\frac{e_{expansion}}{dT} = L\frac{dn}{dT} + (n-1)\alpha L \tag{7.31}$$

For the polarizing beamsplitter the tolerance on the size is +0 -0.2 mm and the material is N-SF1 with a refractive index of 1.68 a thermo-optic coefficient of $0.0 \times 10^{-6}\,\mathrm{K}^{-1}$ a CTE of $9.1 \times 10^{-6}\,\mathrm{K}^{-6}$ giving a $1.2\,\mathrm{nmK}^{-1}$ thermal error for the PBS. The effect due to the cement layer being passed four more times by one signal with respect to the other is also taken into account in this error source as the thickness tolerance is specified with the cement layer already in place.

For the QWP there is no tolerance on the thickness of the glass plate specified, given the nominal thickness of 3.2 mm a tolerance of 0.1 mm or better can be assumed. The material is N-BK7 with a refractive index of 1.5 for

light with a 1550 nm wavelength. The thermo-optic coefficient is $2.4 \times 10^{-6}\,K^{-1}$ and the CTE is $7.1 \times 10^{-6}\,K^{-1}$ resulting in a $0.6\,nmK^{-1}$ thermal error per pass of the QWP.

A finite precision in the placement of the reference mirror and the placement of the glass assembly inside the frame can result in a displacement of the virtual thermal reference plane. as the mirror is front surface coated and mounted on the front surface as well the thickness of the mirror does introduce a deviation. The glass assembly is mounted with a thermal center placed at the end of the beamsplitting surface, such that a thermal expansion does not displace the beamsplitter surface. A 0.25 mm tolerance on the placement of the reference mirror with respect to the thermal center and a CTE of the frame of $10.4 \times 10^{-6}\,K^{-1}$ resulting in a $2.6\,nmK^{-1}$ thermal error for the position of the mirror.

Cosine error of the cat's eye retroreflector
The focal distance of the cat's eye retroreflector can change with temperature, the sensor is designed to minimize this change by using thermal compensation. For the contrast reduction a maximum allowed beam tilt of 100 µrad due to the cat's eye defocus is specified. This budget is specified over the temperature range from the alignment temperature of 20 °C to the maximum temperature of 35 °C the resulting thermal cosine error for this extra beam tilt is 10 nm for the 15 K temperature range, resulting in a thermal error of approximately $0.6\,nmK^{-1}$. The thermal compensation should be better then 17 µm over the temperature range for a focal distance of 46 mm.

Error source	thermal error per degree K
Deviation in form PBS1	1.2 nm
Mounting tolerance reference mirror	2.6 nm
Difference in thickness QWP's	0.6 nm
Cosine error misalignment	0.6 nm
Total thermal error RSS	2.98 nm

Table 7.6: Error budget for unbalanced thermal expansion

7.4. Assembly and Alignment plan

To create an assembly where the tolerances are met specifying very strict manufacturing tolerances some alignment steps can be added to compensate for the tolerance trains due to manufacturing.

In this section the required alignment steps are shown schematically, specifying the alignment resolution and stroke togheter with a method to provide feedback during alignment.

7.4.1. Cat's eye focus

The focus of the cat's eye lens is an active alignment step as the focal distance of the lens can vary from lot to lot for of the shelf lenses and the mechanical tolerances are preferably significantly lower than the tolerance on defocus. A setup as indicated in 7.8 can be used to check the parallelism between the incoming an returning beam. The beamsplitter is positioned such that the returning beam does not travel through the beamsplitter before being incident on the retroreflector. By doing two position measurements of the beams at two different locations the angle of the beams with respect to each other can be determined. For this setup it is important that the two PSD's are mounted in the same plane to reduce the sensitivity to a tilt of the beamsplitter and psd assembly. The accuracy of this setup is limited to the accuracy of the cube corner retroreflector, which has a parallelism better than 15 µrad and the resolution of the PSD's which have a resolution of 5 µm [43**?**]. With this setup an parallelism of 100 µrad can be achieved requiring an actuation in the order of 10 µm, which can be done by using a Nanoflex stage from Thorlabs [41].

7.4.2. Beamsplitter alignment

The second alignment is the mounting of both polarizing beamsplitters with respect to each other. A rotation about the optical axis causes a polarization crosstalk similar to the crosstalk of the finite extinction ratio of PBS2, as this is a compensated error some error may be left after alignment. To create an error equal than the finite extinction ration of the PBS itself the alignment should be better than 30 mrad. As both the beamsplitters are made as a combination of two prisms the side of the PBS may not be perfectly flat, with the dimension tolerance of - 0.25 mm over a 12.7 mm side the alignment can be off by 40 m in worst case. In order

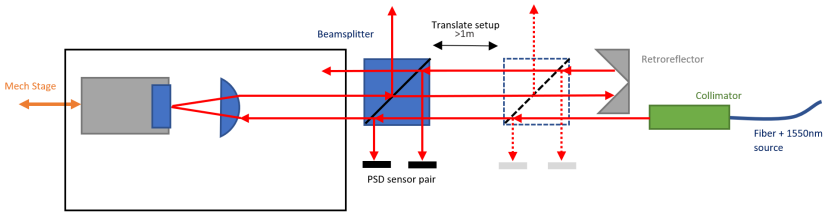

Figure 7.8: The alignment of the cat's eye focal distance. The insert with the mirror is moved such that the returning signal is parallel with the incident light. Two PSDs are used to check the distance between the retro-reflected returning light and the incident light at two distinct locations.

to limit the magnitude of the error PBS2 is actively aligned before being glued together to the glass spacer and PBS1. This alignment can be done to 3 mrad such that the alignment does not cause any significant contribution to the error.

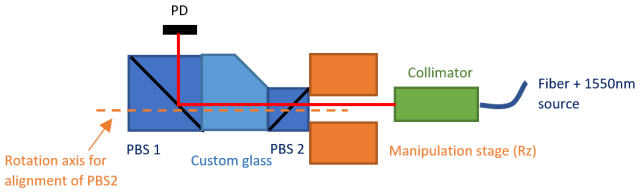

Figure 7.9: Alignment of the polarization axis of the two PBS with respect to each other, the light is polarized by the first PBS and the light should pass through the second PBS, the first PBS is aligned to minimal signal intensity on the photodiode.

7.4.3. QWP alignment

For the alignment of the QWP first a linear polarizer is aligned with the PBS to create a linear polarization state with a higher degree of polarization than the PBS does. Then the QWP is mounted in the manual stage. The motorized stage rotates at a constant frequency such that the polarization state after the QWP can be measured on an oscilloscope. If the polarization state is elliptical the rotating linear polarization creates an AC signal on the photodetector, if the polarization state is perfectly circular the amplitude of this AC signal diminishes and only a DC signal is visible. By keeping the rotation speed at a constant value a filter can be used to reduce the sensitivity to unwanted disturbances during the alignment. A QWP in double pass with a mirror can be seen as the same effect of a half waveplate, which rotates the polarization by twice its own rotation. The signal crosstalk due to a misaligned linear polarization can be expressed in equation 7.32 where E_0 is the original field amplitude and E_{err} is the amplitude of the unwanted signal and θ_{QWP} is the angular deviation of the QWP with respect to its intended position.

$$\frac{E_{err}}{E_0} = \sin 2\theta_{QWP} \tag{7.32}$$

For the alignment to not introduce a significant non linearity error the error signal should be lower than one tenth of the error signal due to the finite retardance accuracy. $\frac{E_{err}}{E_0}$ should be lower than 0.0063 which results in a 3 mrad tolerance for this alignment.

7.4.4. Collimator 1 alignment

The first collimator is aligned to create a beam exiting the sensor head perpendicular to the mounting surface and to create a maximal intensity signal on the photodiode. By aligning the collimators after all components are placed in the interferometer the tolerance stack for the mounting of the other components should only stay within the alignment stroke of this step and therefore the tolerances can be relaxed for manufacturing.

The collimator is held with an manipulator, as there is an Hexapod available that can be used with a mount for the collimator. The collimator is first aligned to exit the sensor perpendicular. This alignment is checked by mounting the sensor head on a jig with a perpendicular guide rail. Then a PSD is placed in front of the sensor head, and this PSD is moved along the guide rail to determine the position of the beam along the path.

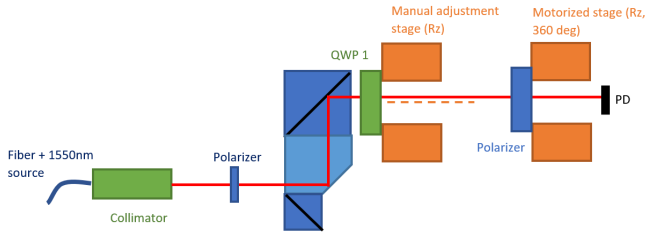

Figure 7.10: Alignment of the quarter waveplate to the polarization state of the PBS, first the light is polarized by a linear polarizer, this polarizer is aligned to the reflected polarization of the PBS to create a linear polarization, hereafter the quarterwaveplate is inserted and the second polarizer is rotated by the motorized stage to create a polarization map. The quarter waveplate is placed such that the resulting polarization is circular.

This setup is shown in figure 7.11 The lateral displacement with respect to the distance gives an misalignment angle. The first reference signal travels to the reference mirror and to the first photodiode through the interferometer optics, this signal can be used to align the collimator for the translations by searching for the maximal signal intensity. This optical path is shown in figure 7.12. As the reference mirror is placed in the virtual retroreflector plane of the cat's eye retroreflector an rotation does not cause beam shear, and the position of the spot for the reference signal corresponds to the position for the spot for a perfectly aligned target mirror. At this location the collimator is locked by injecting a dual cure glue and curing this glue by UV light.

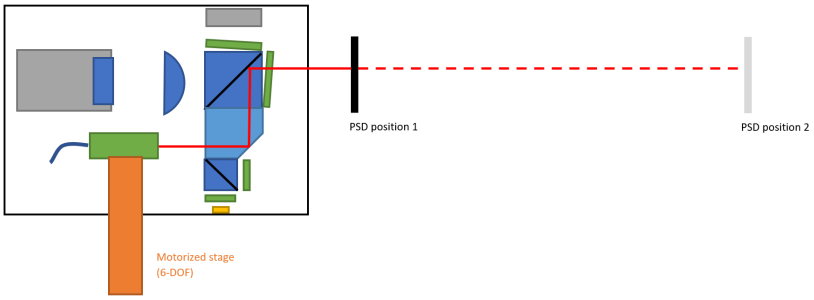

Figure 7.11: Alignment of the first collimator, the sensor head is placed inside a jig with a guidance rail attached to it, the PSD is moved along the guidance rail to check the position of the spot at different distances, the collimator is rotated such that the resulting beam exits the sensor head as perpendicular as possible.

7.4.5. Second collimator alignment

The alignment of the second collimator is done to reduce the wavefront tilt and the wavefront displacement such that the interference contrast is maximum for an unrotated target mirror. An external reference mirror is placed at the virtual retroreflection plane, at the point where the second photodiode would be placed the light exits the sensor head and a non polarizing beamplitter is placed. Close to the beamsplitter a PSD is placed and at a significant distance behind the beamsplitter a second PSD is placed. By switching the laser signal to one collimator at a time the position of one spot at each PSD can be determined, if the laser signal is then send through the other collimator the spot position of the light exiting the second collimator can be seen on both PSD's. First the collimator is rotated such that the the distance between the spots on the PSD's is equal, if this is the case both signals are parallel and the collimator is translated such that the lightbeams overlap.

Again the collimator is locked in place by a double cure adhesive which is cured by UV light.

With the use of the CONEX PSD10GE the spot position can be determined with 5 µm resolution [23], with a 1 m distance between the PSD's the the angle can be determined with a 5 µrad resolution and the beam overlap can be determined by the PSD resolution. The available PI Hexapod has minimal incremental motions of 0.2 µm for x and y translations and 0.08 µm for z translations. For the rotations the minimal incremental motions are respective 2.5 µm and 5 µm for Rx and Ry and R [28]. This setup can therefore be used to create an alignment in the order of 50 µrad. Leaving 50 µrad budget for drift due to glue curing.

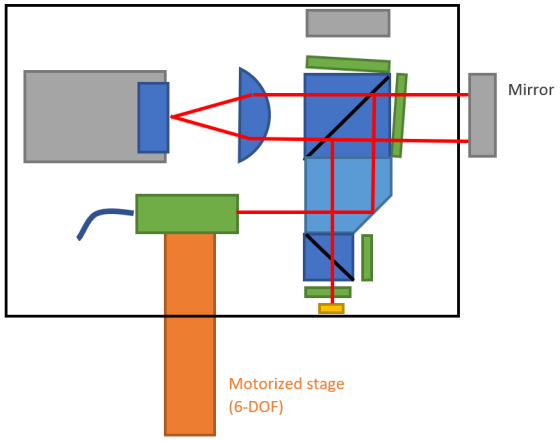

Figure 7.12: The reference signal follows the signal path towards the photodetector, the collimator is now placed such that a maximum intensity is detected at the photodiode.

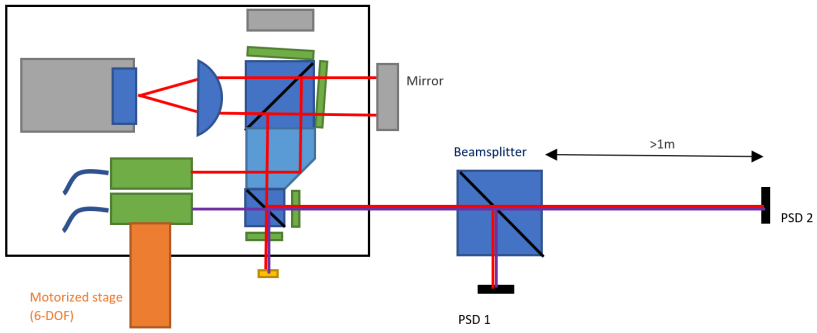

Figure 7.13: The second collimator is aligned such that the signal from the first collimator and the second collimator are parallel and coincident. Both signals are turned on and off one after each other and the spot positions are checked at two locations with PSDs.

7.4.6. Photodiode 2 alignment

The last step is the placement of the second photodiode. As the tolerance train on the thickness of the PBS's adds up to a displacement of PBS2 and therefore the mirror plane between the photodiodes and both collimators are aligned to have maximal signal at the first photodiode the second photodiode is actively aligned by placing it with an external manual stage and locking it with two screws over which a torque relieve plate is positioned.

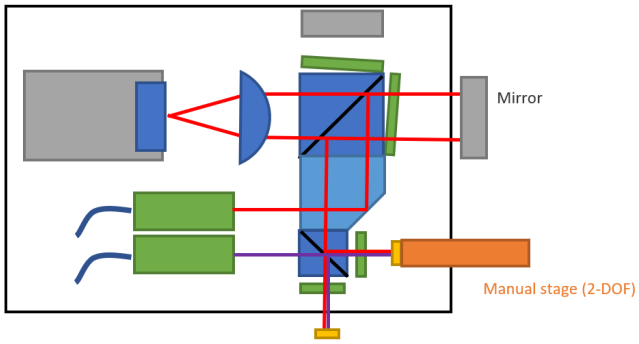

Figure 7.14: The second photodiode is placed at the location where the maximum signal intensity is found. Any one of the two signals from can be used for this alignment.

8

Conclusion and recommendations

Conclusion

A novel source concept is presented which deminishes the inter axis dependency between multiple measurement axis which is present in a fiber fed DFB laser interferometer. By adding a delay line the relative change in modulation depth can be minimized which gives the possibililty to set the laser modulation to a static value for a known range. Therefore eliminating the dependency of the range of the secondary axis on the target distance of a master axis. As a result the interferometer is suitable to measure multiple independent degrees of freedom at the same time.

The introduction of the delay line requires a novel sensor head design, four suitable concepts are presented. The concept that can be built with mostly off the shelf parts is designed in more detail to create a demonstrator for this source concept. The designed sensor head has a 0.73 nm non linearity error, a thermal error of 2.98 nm/K, the noise contribution of the photodiode is insignificant for the systems position noise. These specifications are met with all off the shelf optics except for a glass spacer with a right angle prism to create a preferred form factor. The sensor can work in a low vacuum environment however the focal distance of the cat's eye retroreflector changes and this introduces a cosine error in the measurement, with calibration this error can be corrected for.
By placing the photodiodes on board the interferometer only a single optical vacuum feedthrough is necessary if the fiber splitter is placed in the vacuum and two if the splitter is placed outside the vacuum additionally the common path which introduces speed dependent errors is minimized. No lifetime limiting components are placed inside the sensor head, by using a low power laser source the effect no detrimental effect on the optical coatings is created. With an alignment procedure the tolerance on the mechanical parts are relaxed making these parts relative easy to produce. The size of the interferometer is approximately twice the nice to have. If more custom parts would be used the interferometer could be smaller in size. Therefore the presented sensor head fullfills all the requirements and almost all nice to haves.

The error signal due to the polarization change in the cat's eye retroreflector for a finite spot size is significant and is reduced by reducing the contrast of the interference in the sensor head, a platinum coated CCR would have been better suited as a retroreflector for lower errors and lesser alignment steps.

Recommendations

The concept for the delay line together with the concepts for the sensor heads presented in this thesis can be used as a starting point for further development of low cost high precision interferometers. More research for smaller sensor heads with less optical components and preferably little to no alignment procedures could lead to a broader application for high precision measurement.

Bibliography

[1] Evolving environmental requirements for lithography manufacturing. URL https://www.praecis.com/environmental-control-for-lithography.

[2] *Planar DLA Series*. Aerotech, Inc., 2021. URL https://www.aerotech.com/wp-content/uploads/2021/01/planardla.pdf.

[3] *Planar HDX Series*. Aerotech, Inc., 2021. URL https://www.aerotech.com/wp-content/uploads/2021/01/planarhdx.pdf.

[4] *Displacement Measuring Interferometer*. Attocube systems AG, 2019. URL https://www.attocube.com/downloads/displacement-measuring-interferometer.pdf.

[5] Walter Augustyn and Paul Davis. An analysis of polarization mixing errors in distance measuring interferometers. *Journal of Vacuum Science & Technology B: Microelectronics Processing and Phenomena*, 8 (6):2032–2036, 1990. doi: 10.1116/1.584868.

[6] Norman Bobroff. Recent advances in displacement measuring interferometry. *Measurement Science and Technology*, 4(9):907, 1993. doi: 10.1088/0957-0233/4/9/001.

[7] Hae Young Choi, Kwan Seob Park, Seong Jun Park, Un-Chul Paek, Byeong Ha Lee, and Eun Seo Choi. Miniature fiber-optic high temperature sensor based on a hybrid structured fabry–perot interferometer. *Optics letters*, 33(21):2455–2457, 2008. doi: 10.1364/ol.33.002455.

[8] Suzanne J.A.G. Cosijns, Maarten J. Jansen, and Han Haitjema. Advanced optical incremental sensors: Encoders and interferometers. In Stoyan Nihtianov and Antonio Luque, editors, *Smart Sensors and MEMs (Second Edition)*, Woodhead Publishing Series in Electronic and Optical Materials, pages 245–290. Woodhead Publishing, second edition edition, 2018. ISBN 978-0-08-102055-5. doi: 10.1016/B978-0-08-102055-5.00010-3.

[9] Paul D Hale and Gordon W Day. Stability of birefringent linear retarders (waveplates). *Applied optics*, 27 (24):5146–5153, 1988. doi: 10.1364/AO.27.005146.

[10] Kevin Harding. *Handbook of optical dimensional metrology*. CRC Press, 2013. ISBN 9780429064739. doi: 10.1201/b13855.

[11] Parameswaran Hariharan. *Basics of interferometry*. Elsevier, 2010.

[12] Wenjun He, Fu Yuegang, Yang Zheng, Lei Zhang, Jiake Wang, Zhiying Liu, and Jianping Zheng. Polarization properties of a corner-cube retroreflector with three-dimensional polarization ray-tracing calculus. *Applied optics*, 52:4527–4535, 07 2013. doi: 10.1364/AO.52.004527.

[13] Peter L. M. Heydemann. Determination and correction of quadrature fringe measurement errors in interferometers. *Appl. Opt.*, 20(19):3382–3384, Oct 1981. doi: 10.1364/AO.20.003382.

[14] Pengcheng Hu, Yue Wang, Haijin Fu, Jinghao Zhu, and Jiubin Tan. Nonlinearity error in homodyne interferometer caused by multi-order doppler frequency shift ghost reflections. *Optics express*, 25(4): 3605–3612, 2017. doi: 10.1364/OE.25.003605.

[15] Ki-Nam Joo, Jonathan D Ellis, Eric S Buice, Jo W Spronck, and Robert H Munnig Schmidt. High resolution heterodyne interferometer without detectable periodic nonlinearity. *Optics express*, 18(2):1159–1165, 2010. doi: 10.1364/OE.18.001159.

[16] Ki-Nam Joo, Erin Clark, Yanqi Zhang, Jonathan D Ellis, and Felipe Guzmán. A compact high-precision periodic-error-free heterodyne interferometer. *JOSA A*, 37(9):B11–B18, 2020. doi: 10.1364/JOSAA.396298.

[17] Ralph Kalibjian. Polarization preserving corner cubes. *Optics & Laser Technology*, 44(1):239–246, 2012. doi: 10.1016/j.optlastec.2011.06.025.

[18] *Optics and Laser Heads for Laser-Interferometer Positioning Systems*. Keysight Technologies, 2017. URL https://www.keysight.com/nl/en/assets/7018-06711/technical-overviews/5964-6190.pdf.

[19] Bastiaan Andreas Wilhelmus Hubertus Knarren. *Application of optical fibres in precision heterodyne laser interferometry*. PhD thesis, 2003.

[20] O Kruger and N Chetty. Robust air refractometer for accurate compensation of the refractive index of air in everyday use. *Applied optics*, 55(32):9118–9122, 2016.

[21] Rainer Köning, Gejza Wimmer, and Viktor Witkovský. Ellipse fitting by nonlinear constraints to demodulate quadrature homodyne interferometer signals and to determine the statistical uncertainty of the interferometric phase. *Measurement Science and Technology*, 25:115001, 10 2014. doi: 10.1088/0957-0233/25/11/115001.

[22] Hakchu Lee. Optical thin films on polarization preserving cube corner retroreflectors. In *Advances in Optical Thin Films III*, volume 7101, page 710112. International Society for Optics and Photonics, 2008. ISBN 9780819473318.

[23] *Position sensing detector, Conex PSD series*. Newport Corperation, 2015. URL https://www.newport.com/mam/celum/celum_assets/np/resources/Conex_PSD_Series-Update.pdf?0.

[24] Juichi Noda, Katsunari Okamoto, and Yutaka Sasaki. Polarization-maintaining fibers and their applications. *Journal of Lightwave Technology*, 4(8):1071–1089, 1986. doi: 10.1109/JLT.1986.1074847.

[25] Fabián E Peña-Arellano and Clive C Speake. Mirror tilt immunity interferometry with a cat's eye retroreflector. *Applied optics*, 50(7):981–991, 2011.

[26] *A-322 PIglide HS Planar Scanner with Air Bearing*. Physik Instrumente (PI) GmbH & Co. KG, 2020. URL https://www.physikinstrumente.com/en/products/xy-stages/a-322-piglide-hs-planar-scanner-with-air-bearing-900713/.

[27] *V-741 High-Precision XY Stage*. Physik Instrumente (PI) GmbH & Co. KG, 2020. URL https://www.physikinstrumente.com/en/products/xy-stages/v-741-high-precision-xy-stage-412418441/#specification.

[28] *H-811.I2 Datasheet*. Physik Instrumente (PI) GmbH & Co. KG, 2021. URL https://static.physikinstrumente.com/fileadmin/user_upload/physik_instrumente/files/datasheets/H-811.I2-Datasheet.pdf.

[29] TS Priest, KT Jones, GB Scelsi, and GA Woolsey. Thermal coefficients of refractive index and expansion in optical fibre sensing. In *Optical Fiber Sensors*, page OWC41. Optical Society of America, 1997.

[30] *RLE system performance*. Renishaw plc, 2017. URL http://resources.renishaw.com/en/download/data-sheet-rle-system-performance--93259. A.

[31] Vidi Saptari. *Fourier transform spectroscopy instrumentation engineering*. SPIE Optical Engineering Press Bellingham Washington, DC, 2003. ISBN 9780819478672.

[32] *Stress in optical glass*. Schott AG, 2019. URL https://www.schott.com/d/advanced_optics/1275dc1e-ef01-45d1-a88a-79deec322443/1.8/schott_tie-27_stress_in_optical_glass.pdf.

[33] Sidney A Self. Focusing of spherical gaussian beams. *Applied optics*, 22(5):658–661, 1983.

[34] Robert R Shannon. *The art and science of optical design*. Cambridge University Press, 1997.

[35] *Specification sheet*. SmarAct GmbH, 2021. URL https://www.smaract.com/files/media/categories/Optical%20Metrology/Spec-Sheets/PS-SS00020_PSV2-SpecSheet.pdf.

[36] JJ Snyder. Paraxial ray analysis of a cat's-eye retroreflector. *Applied optics*, 14(8):1825–1828, 1975. doi: 10.1364/AO.54.007387.

[37] Jingming Song, Kang Sun, Shuai Li, and Wei Cai. Phase sensitivity to temperature of the guiding mode in polarization-maintaining photonic crystal fiber. *Applied optics*, 54(24):7330–7334, 2015.

[38] Clive C Speake and Miranda J Bradshaw. Pseudo-cat's eye for improved tilt-immune interferometry. *Applied optics*, 54(24):7387–7395, 2015. doi: 10.1364/AO.50.000981.

[39] William C Swann and Sarah L Gilbert. Line centers, pressure shift, and pressure broadening of 1530-1560 nm hydrogen cyanide wavelength calibration lines. *JOSA B*, 22(8):1749–1756, 2005.

[40] *FGA21 spec sheet*. Thorlabs Inc., . URL https://www.thorlabs.com/drawings/93d590a92bc7eb47-00687688-F06B-98CC-9572B68CC1A43EA6/FGA21-SpecSheet.pdf.

[41] *Single-Axis Flexure Translation Stages: 5 mm Travel*. Thorlabs Inc., . URL https://www.thorlabs.com/newgrouppage9.cfm?objectgroup_id=720.

[42] *Polarization-Maintaining FC/APC Fiber Optic Patch Cables*. Thorlabs Inc., . URL https://www.thorlabs.com/newgrouppage9.cfm?objectgroup_id=3345.

[43] *TIR retroreflector prisms*. Thorlabs Inc., . URL https://www.thorlabs.com/newgrouppage9.cfm?objectgroup_id=145.

[44] *Optical coatings - AR coatings*. Thorlabs Inc., . URL https://www.thorlabs.com/newgrouppage9.cfm?objectgroup_id=5840.

[45] *Laser line beamsplitters*. Thorlabs Inc., . URL https://www.thorlabs.com/newgrouppage9.cfm?objectgroup_id=7490.

[46] *25.4 mm Polarizing beamsplitter 1200-1600 nm*. Thorlabs Inc., 2014. URL https://www.thorlabs.com/drawings/93d590a92bc7eb47-00687688-F06B-98CC-9572B68CC1A43EA6/PBS254-AutoCADPDF.pdf.

[47] *Liquid crystal polymer quarter-waveplate*. Thorlabs Inc., 2018. URL https://www.thorlabs.com/drawings/93d590a92bc7eb47-00687688-F06B-98CC-9572B68CC1A43EA6/WPQ10E-1550-AutoCADPDF.pdf.

[48] *MOUNTED ZERO-ORDER COMPOUND WAVE PLATE*. Thorlabs Inc., 2018. URL https://www.thorlabs.com/drawings/93d590a92bc7eb47-00687688-F06B-98CC-9572B68CC1A43EA6/WPQ10M-1550-AutoCADPDF.pdf.

[49] *FC/APC collimation package 1550nm*. Thorlabs Inc., 2021. URL https://www.thorlabs.com/drawings/93d590a92bc7eb47-00687688-F06B-98CC-9572B68CC1A43EA6/F280APC-1550-AutoCADPDF.pdf.

[50] Klaus Thurner, Pierre-François Braun, and Khaled Karrai. Fabry-pérot interferometry for long range displacement sensing. *Review of Scientific Instruments*, 84(9):095005, 2013. doi: 10.1063/1.4821623.

[51] Klaus Thurner, Francesca Paola Quacquarelli, Pierre-François Braun, Claudio Dal Savio, and Khaled Karrai. Fiber-based distance sensing interferometry. *Applied optics*, 54(10):3051–3063, 2015. doi: 10.1364/AO.54.003051.

[52] *DFB – Distributed Feedback Diodes*. Toptica photonics, 2021. URL https://www.toptica.com/products/laser-diodes/dfbdbr/.

[53] Jennifer Watchi, Sam Cooper, Binlei Ding, Conor M Mow-Lowry, and Christophe Collette. Contributed review: A review of compact interferometers. *Review of Scientific Instruments*, 89(12):121501, 2018. doi: 10.1063/1.5052042.

[54] *Data HCN*. Wavelengthreferences.com, 2021. URL https://www.wavelengthreferences.com/wp-content/uploads/Data-HCN.pdf.

[55] K. J. Wayne. High thermal stability plane mirror interferometer, jun 1988. US Patent 4784490A.

[56] Jay H. Zimmerman and Jack A. Stone. *Index of Refraction of Air*. National Institute of Standards and Technology, 2001. URL `https://emtoolbox.nist.gov/Wavelength/Documentation.asp#EdlenorCiddor`.

[57] *ZMI High Stability Plane Mirror Interferometer (HSPMI)*. Zygo Corporation, 2009. URL `https://www.zygo.com/support/reference-library/brochures-and-specsheets`.